

Non-Gaussian Halo Mass Function and Non-Spherical Halo Collapse: Theory vs. Simulations

Ixandra E. Achitouv* & Pier Stefano Corasaniti*

*Laboratoire Univers et Théories (LUTh),
UMR 8102 CNRS, Observatoire de Paris, Université Paris Diderot,
5 Place Jules Janssen, 92190 Meudon, France

E-mail: Ixandra.Achitouv@obspm.fr, Pier-Stefano.Corasaniti@obspm.fr

Abstract. The mass distribution of dark matter halos is a sensitive probe of primordial non-Gaussianity (NG). We derive an analytical formula of the halo mass function by perturbatively computing excursion set path-integrals for a non-Gaussian density field with non-vanishing skewness, f_{NL} . We assume a stochastic barrier model which captures the main features of the ellipsoidal collapse of halos. Contrary to previous results based on extensions of the Press-Schechter formalism to NG initial conditions, we find that the non-spherical collapse of halos directly alter the signature of primordial NG. This points toward a potential degeneracy between the effect of primordial non-Gaussianity and that of non-linear halo collapse. The inferred mass function is found to be in remarkable agreement with N-body simulations of NG local type. Deviations are well within numerical uncertainties for all values of f_{NL}^{loc} in the range of validity of the perturbative calculation ($|f_{nl}^{loc}| \lesssim 200$). Moreover, the comparison with simulation results suggests that for $|f_{NL}| \gtrsim 30$ the non-linear collapse of halos, as described by our barrier model, strongly deviates from that of Gaussian initial conditions. This is not surprising since the effect of non-linear gravitational processes may be altered by initially large NG. Hence, in the lack of prior theoretical knowledge, halo collapse model parameters should be included in statistical halo mass function data analysis which aim to constrain the signature of primordial NG.

Keywords: Cosmology, Non-Gaussianity, Halo Mass Function

Contents

1	Introduction	1
2	Excursion Set Theory	4
2.1	Correlated Random Walks and Halo Mass	4
2.2	Stochastic Barrier and Ellipsoidal Collapse	5
2.2.1	State of art of the stochastic barrier model	5
2.2.2	Modelisation of the Diffusing Drifting Barrier	6
2.3	Path-Integral Formulation	7
2.4	Gaussian Halo Mass Function	9
3	Non-Gaussian Halo Mass Function	11
3.1	Leading Term	12
3.2	Next-to-Leading Term	13
4	Local and Equilateral Non-Gaussian Mass Function	15
4.1	Reduced bispectra and fitting functions	15
4.2	Validity of the perturbative expansions	17
4.2.1	Limits on the mass range	18
4.2.2	Limits on f_{NL}	19
5	Halo Collapse Model and NG Signal	20
6	NG Halo Mass Function and N-body Simulations	22
7	Conclusion	26

1 Introduction

The statistics of the primordial density fluctuation field carries unique information on the physics of the very early Universe. Standard slow-roll inflation predicts a nearly scale invariant spectrum of Gaussian, adiabatic density perturbations [1–7]. Alternatively, high-energy physics inspired scenarios may leave large non-Gaussian signatures on the initial matter density distribution [8–19]. Hence, the detection of primordial non-Gaussianity (NG) has the potential to disclose quantum physical processes at energies which are out of reach of laboratory experiments. In recent years this has motivated a revived interest on testing the Gaussian hypothesis through measurements of the high-order angular correlation functions of the Cosmic Microwave Background (CMB) anisotropies [20–23].

The quest for primordial NG has primarily focused on the amplitude and shape of the CMB bispectrum statistics [24–27]. The next generation of cosmic structure surveys may also provide complementary constraints, since the spatial distribution of

galaxies in the universe carries an imprint of the statistics of the initial matter density fluctuations. As shown in several studies, measurements of the galaxy bispectrum [28–32] and the abundance of galaxy clusters [33–35] are sensitive NG probes. However, an accurate modeling of the non-linear regime of gravitational collapse is necessary for such tests to be successful. This is because the late time non-linear evolution of density perturbations induces strong non-Gaussian features in the spatial distribution of cosmic structures, thus potentially obscuring the imprint of primordial non-Gaussianity. Accounting for these effects is the premise to testing the statistics of the initial density field.

In this context the determination of the mass distribution of dark matter halos is of primary importance. Halos are gravitationally bound objects resulting from the non-linear collapse of dark matter perturbations. It is inside these virialized structures that cooling baryonic gas falls in to form the stars and galaxies that we observe today. Numerical N-body simulations have been extensively used to study the non-linear clustering of matter in the standard cosmological scenario with Gaussian initial conditions. On the other hand, simulations with non-Gaussian initial conditions have become available only in the past few years (e.g., see refs. [36–39]). This has driven a major effort toward formulating a mathematical model description of the NG halo mass distribution. A number of studies have approached this problem by extending the original Press-Schechter (PS) derivation to NG initial conditions. The seminal work by Press and Schechter [40] has provided the first formal derivation of the halo abundance in the case of an initial Gaussian density field. The basic idea is that halos form in regions of the linear density field smoothed on a given scale R (associated to a mass M), whose density lies above a critical threshold of collapse (e.g. δ_c the linearly extrapolated spherical top-hat density perturbation at the time of collapse [41]). Using such a prescription, the fraction of mass in halos with mass $> M$ is given by

$$F(> M) = \int_{\delta_c}^{\infty} \Pi(\delta, M) d\delta, \quad (1.1)$$

where $\Pi(\delta, M)$ is the probability distribution of the smoothed linear density field. Then, the number density of halos with mass in the range $[M, M + dM]$ is obtained by equating

$$\frac{dn}{dM} = \frac{\bar{\rho}}{M} \frac{dF}{dM}, \quad (1.2)$$

with $\bar{\rho}$ being the mean background matter density.

The computation can be extended to non-Gaussian initial conditions by specifying the form of $\Pi(\delta, M)$. For example, Matarrese, Verde and Jimenez [42] have written $\Pi(\delta, M)$ as a path-integral of an infinite series of cumulants of the density field δ . This allowed them to derive an approximate formula for dn/dM in the limit of small NG up to leading order in the skewness parameter, f_{NL} . Similarly, in [43] the authors have approximated $\Pi(\delta, M)$ as an Edgeworth expansion in the cumulants and truncated the series to infer an expression of the mass function which explicitly depends on f_{NL} (for an extension to the ellipsoidal collapse threshold see ref. [44]). Overall these studies have provided indications of how primordial NG affects the halo mass distribution.

However, by relying on the PS approach they have failed to address a number of important issues that are the main limitation of the PS formalism. As an example in Press-Schechter the normalization factor of the mass function is related to the “cloud-in-cloud” problem. Namely, the fact that a collapsed region of mass M contributes to the halo mass counting only if it is not embedded in a collapsed region of greater mass $M' > M$. The PS formalism does not address this issue, thus miscounting the fraction of mass in halos. Moreover, even including an ad-hoc correction to recover the correct normalization, the PS formula still fails to reproduce results from N-body simulations. Because of this, analyses based on the PS approach have mainly focused on predicting the ratio of the non-Gaussian to Gaussian Press-Schechter mass function and normalized the result with a fitting function to Gaussian N-body simulation data. A recent comparison with non-Gaussian simulations indicates that these analytical formulae are in relatively good agreement with numerical results provided an ad-hoc rescaling of the spherical collapse threshold is assumed [37].

Ideally, one would like to perform an *ab initio* calculation to consistently account for the cloud-in-cloud problem as well as the non-spherical collapse of halos for any type of initial conditions. The excursion set theory introduced by Bond et al. [45] provides a powerful mathematical framework capable of addressing these issues and allowing for a self-consistent derivation of the mass function from a limited set of initial assumptions. The formalism frames the original Press-Schechter idea in the context of stochastic calculus. However, the difficulty in obtaining analytical solutions for realistic description of halos has been the main limitation of the theory (for a review see ref. [46]). In fact, in the case of a Gaussian field an analytic treatment is possible only if one assume an unphysical halo mass definition. The computation for a realistic case requires to solve numerically the stochastic model equations through time consuming Monte Carlo simulations (see e.g. refs. [45, 47]).

In a series of papers Maggiore & Riotto [48–50] have introduced a path-integral description of the excursion set which allows for a perturbative calculation of the mass function in the case of physical mass definitions. Non-Gaussian initial conditions can be easily implemented in this novel formulation as well as more realistic conditions for the gravitational collapse of halos. This has provided a major breakthrough towards an accurate physical model description of the mass function. For instance, in [51, 52] we have implemented such an approach with an effective stochastic barrier model which accounts for the main characteristics of the ellipsoidal collapse of halos. This has allowed us to derived an analytic formula which shows an unprecedented agreement with the mass function from Gaussian N-body simulations.

In this paper we extend the study of the non-spherical collapse mass function to the case of primordial non-Gaussianity. Our goal is to derive a better understanding of how the halo collapse alters the signature of primordial NG and confront the theoretical model prediction against non-Gaussian N-body simulation results. The paper is organized as follows: in section 2 we introduce the excursion set theory, the path-integral formalism and discuss diffusive drifting barrier model of halo collapse. In section 3 we derive the non-Gaussian mass function and shown its application to local and equilateral non-Gaussianity in section 4. We discuss the imprints on the halo mass function

due to primordial NG and the halo collapse model in section 5, while in section 6 we present the results of the comparison to non-Gaussian N-body simulations. Finally we discuss the conclusions in section 7.

2 Excursion Set Theory

2.1 Correlated Random Walks and Halo Mass

Let us consider a non-Gaussian density field $\delta(\mathbf{x})$ smoothed on a scale R :

$$\delta(\mathbf{x}, R) = \frac{1}{(2\pi)^3} \int d^3k \tilde{W}(k, R) \tilde{\delta}(\mathbf{k}) e^{-i\mathbf{k} \cdot \mathbf{x}} \quad (2.1)$$

where $\tilde{W}(k, R)$ is the Fourier transform of the filter function in real space, $W(x, R)$. The latter defines the mass inside a region of radius R as $M = \bar{\rho}V(R)$, with $\bar{\rho}$ being the mean background density and $V(R) = \int d^3x W(x, R)$ is the filtered volume. Then, the variance of the smoothed density field reads as

$$S = \langle \delta^2(R) \rangle \equiv \sigma^2(R[M]) = \frac{1}{2\pi^2} \int dk k^2 P(k) \tilde{W}^2[k, R(M)], \quad (2.2)$$

where $P(k)$ is the linear matter power spectrum at redshift $z = 0$. Given the one-to-one relation between smoothing radius, mass and variance, we can rewrite the halo mass function eq. (1.2) as

$$\frac{dn}{dM} = f(\sigma) \frac{\bar{\rho}}{M^2} \frac{d \log \sigma^{-1}}{d \log M}, \quad (2.3)$$

where $f(\sigma) = 2\sigma^2 \mathcal{F}(\sigma^2)$ is the so called ‘‘multiplicity function’’ and $\mathcal{F}(S) = dF/dS$ is the derivative of the fraction of mass in halos with mass $> M[S]$. The goal of the excursion set theory is to calculate $f(\sigma)$ from $\mathcal{F}(S)$ obtained as the first up-crossing distribution of the random walks $\delta(\mathbf{x}, R)$ as function of the smoothing radius $R[S]$ (or equivalently S , which plays the role of pseudo-time). Trajectories starts at $S = 0$ (i.e. large radii limit $R \rightarrow \infty$) with $\delta_0 = 0$. The fraction of mass in halos is then inferred from counting the rate at which trajectories hit for the first time an absorbing barrier. The mass function at high redshifts can be inferred by simply rescaling all linear quantities by the growth factor predicted by the cosmological model under consideration.

The nature of the random walks depends on the statistics of the initial density field as well as the form of the filter function. In the case of a sharp-k filter, $W(k, R) = \theta(1 - kR)$, the random walks are Markovian with $\langle \delta(S)\delta(S') \rangle_c = \min(S, S')$.¹ In such a case the first-crossing distribution is obtained by solving a simple Fokker-Planck diffusion problem. However, the sharp-k filtering does not correspond to a physical halo mass, since the filtered volume $V(R)$ is undefined (see e.g. discussion in [48]).

¹We use the underscore c to indicated connected correlators.

The only unambiguously defined mass is associated with a top-hat filter in real space, $W(x, R) = \theta(R - x)$ (sharp-x filter) whose Fourier transform reads as

$$\tilde{W}(k, R) = \frac{3}{(kR)^3} [\sin(kR) - (kR) \cos(kR)]. \quad (2.4)$$

In such a case the evolution of the random walks acquires pseudo-time correlations for which to our knowledge an analytical solution of the first-crossing distribution does not exist. Maggiore & Riotto [48] have shown that such correlations can be treated perturbatively around the Markovian solution. In particular, for a sharp-x filter the two point connected correlator can be written as $\langle \delta(S)\delta(S') \rangle_c = \min(S, S') + \Delta(S, S')$, where $\Delta(S, S') \approx \kappa S/S'(S' - S) < 1$ (with $S < S'$) and κ is a small parameter of nearly constant amplitude, whose value depends on the underlying cosmology. For a vanilla Λ CDM model $\kappa \approx 0.475$. Hence, the non-Markovian first-crossing distribution can be inferred as a perturbative expansion in κ .

2.2 Stochastic Barrier and Ellipsoidal Collapse

2.2.1 State of art of the stochastic barrier model

The absorbing barrier is the other crucial ingredient of the excursion set formalism which encodes information on the non-linear collapse of halos. In the spherical collapse model, the barrier is a constant threshold, $B = \delta_c$. However, this model is a too simple description of the collapse of dark matter halos in the universe. The gravitational collapse can be highly non-spherical. As already shown in the seminal work by Doroshkevich [60] perturbations in a Gaussian density field are triaxial and subject to external tidal shear. The implications of this are twofold. First, the collapse of a homogeneous ellipsoid [61] provides a better description of the system. Secondly, the stochastic nature of the underlying density field implies that the parameters characterizing the ellipsoid (ellipticity and prolateness) are random variables with a well defined probability distribution that can be derived from that of the density field. Consequently, the condition of collapse is no longer specified by a unique constant value, but it is a random variable itself [53, 54]. In the excursion set framework this implies treating the barrier as a stochastic variable which performs a random walk whose characteristics are given by the moments of the probability distribution resulting from the ellipsoidal collapse model considered. Unfortunately the full distribution of the barrier remains unset. Most of the work dedicated to the ellipsoidal collapse threshold have limited their analysis to the average behavior of the collapse threshold as function of the halo mass. As an example Sheth, Mo & Tormen found that the average ellipsoidal collapse barrier evolves as $\langle B(S) \rangle = \delta_c(1 + \beta S^\gamma)$. This behavior is consistent with the physical expectation that collapse of small mass halos differ from spherical symmetry. In fact, at large S (small mass) the shear field is higher than at small S (large mass) thus implying that small mass halos need to reach a higher density of collapse than that predicted by the spherical model. However, knowledge of the scatter around this average encodes additional information on the non-linear collapse process. To date the variance of the stochastic barrier has been studied only qualitatively [54]. In [62] it has

been shown that the dynamics of the collapse depends not only on the local properties of the shear field but also on interaction between ellipsoidal perturbations and its large scales environment. One of the key parameter to quantify this effect is the large scale environment density. Low mass haloes are more affected by this large scale environment and one of the consequence is to increase the scatter. This study was done for a Gaussian field but it already suggests that the imprint of the primordial density field is underline at high mass halo while the dynamics and the cosmology dependences induce by the environment dynamics is underline in low mass haloes.

However we must not draw any conclusion on the value of these parameters without a proper account of the "second order cloud in cloud problem". In the excursion set, we assume that we can consider random walks around the same coordinate holding on the ergodic principle. This hypothesis is approximative and it is possible to measure the induced discrepancy on the scatter by doing the analysis of [54]: comparing the scatter for center of mass walk and random particle of the simulation. Nevertheless this will require a dedicated study that we would like to perform in the future including non-Gaussian statistic of the primordial field. In the absence of prescription we focus a simpler model with captures the main feature of the fuzzy barrier.

2.2.2 Modelisation of the Diffusing Drifting Barrier

As we already introduce in [51, 52] we use a stochastic barrier with Gaussian diffusion and linear drifting average, which we refer as the "Diffusive Drifting Barrier" model (DDB). In this model the barrier performs a Markovian random walk starting at $B_0 = \delta_c$ with $\langle B(S) \rangle_c = \delta_c + \beta S$ and $\langle B(S)B(S') \rangle_c = D_B \min(S, S')$. Here β parametrizes the rate at which the collapse threshold on average deviates from the spherical collapse prediction and D_B measures the amplitude of a constant scatter around the average collapse threshold at a given mass scale. The linear behaviour of the average of the threshold approximates the mean value of the Sheth Mo and Tormen ellispoidal barrier in the mass of interest.

Therefore, differently from the linear density field δ , the non-Markovian part of the barrier 2-point connected correlator identically vanishes, $\Delta_B(S, S') = 0$. One may wonder if a better modeling of the stochastic barrier should account for the correlations induced by the filtering process. However, as already pointed out in [52], there is no reason as to why the barrier should have the same filtering of the linear density field, since the two procedures have very different physical meanings. The latter is associated to the halo mass definition, while the former specifies the correlation between the condition of collapse at different scales. To date there is no study that has looked at such correlation in the context of the ellipsoidal collapse model. In the lack of information, the simplest approximation is to assume that the collapse condition at scale S is independent of that at S' , i.e. $\Delta_B(S, S') = 0$. This suggests that in order to improve the modeling of the stochastic barrier one should completely solve the ellipsoidal collapse model through a detailed numerical analysis from which to infer

moments and correlators of the fuzzy barrier. This will also allow to predict the redshift and cosmology dependence of β and D_B .

The stochastic system can be simplified into one-dimensional random walks by introducing the variable $Y = B - \delta$, with initial condition $Y_0 = \delta_c$ and absorbing boundary at $Y_c = 0$. Non-Gaussian initial conditions can be easily included through the higher-order connected correlation functions of the smoothed linear density field. For instance, let us consider non-Gaussianity generated by the three-point correlation function (skewness). In such a case the random walks are completely specified by the non-vanishing connected correlators

$$\langle Y(S) \rangle_c = \delta_c + \beta S, \quad (2.5)$$

$$\langle Y(S)Y(S') \rangle_c = (1 + D_B)\min(S, S') + \Delta(S, S'), \quad (2.6)$$

$$\langle Y(S)Y(S')Y(S'') \rangle_c = -\langle \delta(S)\delta(S')\delta(S'') \rangle_c, \quad (2.7)$$

where $\langle \delta(S)\delta(S')\delta(S'') \rangle_c$ is the three point correlation function of the smoothed linear density field. The goal of the excursion set is to compute $\Pi(Y_0, Y, S)$, the probability distribution of the random walks which start at Y_0 and reach Y at time S obeying eq. (2.5), (2.6) and (2.7), with $\Pi(Y_0, Y_c, S) = 0$. Then, the first-crossing distribution can be derived as

$$\mathcal{F}(S) = -\frac{\partial}{\partial S} \int_{Y_c}^{\infty} dY \Pi(Y_0, Y, S). \quad (2.8)$$

2.3 Path-Integral Formulation

The computation of $\Pi(Y_0, Y, S)$ can be performed using the path-integral method introduced in [48]. Let us consider a discretized interval $[0, S]$ in steps $\Delta S = \epsilon$, such that $S_k = k\epsilon$ with $k = 1, \dots, n$. The probability distribution of the discrete random walks that never cross the barrier reads as

$$\Pi_{\epsilon}(Y_0, Y_n, S_n) = \int_{Y_c}^{\infty} dY_1 \dots \int_{Y_c}^{\infty} dY_{n-1} W(Y_0, \dots, Y_n, S_n), \quad (2.9)$$

where

$$W(Y_0, \dots, Y_n, S_n) \equiv \langle \delta_D(Y(S_1) - Y_1) \dots \delta_D(Y(S_n) - Y_n) \rangle, \quad (2.10)$$

is the probability density distribution. Using the Fourier transform of the Dirac-function we can rewrite eq. (2.10) as

$$W(Y_0, \dots, Y_n, S_n) = \int \mathcal{D}\lambda e^{i\sum_{i=1}^n \lambda_i Y_i} \langle e^{-i\sum_{i=1}^n \lambda_i Y(S_i)} \rangle, \quad (2.11)$$

with $\int \mathcal{D}\lambda = \int_{-\infty}^{\infty} \frac{d\lambda_1}{2\pi} \dots \frac{d\lambda_n}{2\pi}$. As clearly pointed out in [50], the exponential term inside the average is nothing else than the exponential of the partition function, $e^Z = \langle e^{-i\sum_{i=1}^n \lambda_i Y(S_i)} \rangle$. For generic non-Gaussian random walks this reads as

$$Z = \sum_{p=1}^{\infty} \frac{(-i)^p}{p!} \sum_{i_1=1}^n \dots \sum_{i_p=1}^n \lambda_{i_1} \dots \lambda_{i_p} \langle Y_{i_1} \dots Y_{i_p} \rangle_c, \quad (2.12)$$

where $\langle Y_{i_1} \dots Y_{i_p} \rangle_c$ is the p -point connected correlator. Using eq. (2.5), (2.6) and (2.7) and substituting in eq. (2.10) we have

$$\begin{aligned} \Pi_\epsilon(Y_0, Y_n, S_n) &= \int_{Y_c}^\infty dY_1 \dots \int_{Y_c}^\infty dY_{n-1} \int \mathcal{D}\lambda e^{-i\Sigma_k \lambda_k [\bar{B}_k - Y_k] - \frac{1}{2} \Sigma_{ij} \lambda_i \lambda_j A_{ij}} \times \\ &\times e^{-\frac{1}{2} \Sigma_{ij} \lambda_i \lambda_j \Delta_{ij}} e^{\frac{(-i)^3}{6} \Sigma_{ijk} \lambda_i \lambda_j \lambda_k \langle Y_i Y_j Y_k \rangle_c}, \end{aligned} \quad (2.13)$$

with $A_{ij} = \epsilon(1 + D_B) \min(i, j)$. Since $\Delta_{ij} \equiv \Delta(S_i, S_j) < 1$ and assuming small departure from Gaussianity, we can expand the exponentials in eq. (2.13) to first order in Δ_{ij} and $\langle Y_i Y_j Y_k \rangle_c$ respectively. Then using the relation $\lambda_i e^{-i\lambda_i [\bar{B}_i - Y_i]} = -i\partial/\partial Y_i e^{-i\Sigma_k \lambda_k [\bar{B}_k - Y_k]}$ we can write

$$\Pi_\epsilon(Y_0, Y_n, S_n) \approx \Pi_0^\epsilon(Y_0, Y_n, S_n) + \Pi_1^\epsilon(Y_0, Y_n, S_n) + \Pi_{NG}^\epsilon(Y_0, Y_n, S_n), \quad (2.14)$$

where

$$\Pi_0^\epsilon(Y_0, Y_n, S_n) = \int_{Y_c}^\infty dY_1 \dots \int_{Y_c}^\infty dY_{n-1} W_0(Y_0, \dots, Y_n, S_n), \quad (2.15)$$

is the Markovian probability distribution with density

$$W_0(Y_0, \dots, Y_n, S_n) = \int \mathcal{D}\lambda e^{-i\Sigma_k \lambda_k [\bar{B}_k - Y_k] - \frac{1}{2} \Sigma_{ij} \lambda_i \lambda_j A_{ij}}, \quad (2.16)$$

which obeys the Chapman-Kolmogorov equation (see appendix A in ref. [52]),

$$\Pi_1^\epsilon(Y_0, Y_n, S_n) = \frac{1}{2} \sum_{ij} \int_{Y_c}^\infty dY_1 \dots \int_{Y_c}^\infty dY_{n-1} \Delta_{ij} \partial_i \partial_j W_0(Y_0, \dots, Y_n, S_n), \quad (2.17)$$

is the first order correction in κ and

$$\Pi_{NG}^\epsilon(Y_0, Y_n, S_n) = -\frac{1}{6} \sum_{ijk} \langle \delta_i \delta_j \delta_k \rangle_c \int_{Y_c}^\infty dY_1 \dots \int_{Y_c}^\infty dY_{n-1} \partial_i \partial_j \partial_k W_0(Y_0, \dots, Y_n, S_n) \quad (2.18)$$

is the non-Gaussian term [50]. Notice that due to the separate expansions in Δ_{ij} and $\langle Y_i Y_j Y_k \rangle_c$ we have mixing terms. However, as we will discuss later, these are negligible to first order in κ and f_{NL} . By evaluating these integrals in the continuous limit ($\epsilon \rightarrow 0$) and computing the corresponding first-crossing distribution we obtain a mass function that consists of three independent terms

$$f(\sigma) = f_0(\sigma) + f_1(\sigma) + f_{NG}(\sigma), \quad (2.19)$$

where $f_0(\sigma)$ is the Markovian part of the Gaussian mass function, $f_1(\sigma)$ is the non-Markovian correction to the Markovian solution to first order in κ due to the filtering process of the linear density field and $f_{NG}(\sigma)$ is the non-Gaussian contribution. Before presenting the computation of $f_{NG}(\sigma)$, it is worth reviewing the main features of the Gaussian mass function derived in [51, 52].

2.4 Gaussian Halo Mass Function

The Markovian mass function for a diffusive drifting barrier reads as

$$f_0(\sigma) = \frac{\delta_c}{\sigma} \sqrt{\frac{2a}{\pi}} e^{-\frac{a}{2\sigma^2}(\delta_c + \beta\sigma^2)^2}. \quad (2.20)$$

where $a = 1/(1 + D_B)$. The non-Markovian correction due to the filter function is given as an expansion to second order in β

$$f_1(\sigma) = f_{1,\beta=0}^{m-m}(\sigma) + f_{1,\beta(1)}^{m-m}(\sigma) + f_{1,\beta(2)}^{m-m}(\sigma) \quad (2.21)$$

with

$$f_{1,\beta=0}^{m-m}(\sigma) = -a \kappa \sqrt{\frac{2}{\pi}} \frac{Y_0 \sqrt{a}}{\sigma} \left(e^{-\frac{aY_0^2}{2\sigma^2}} - \frac{1}{2} \Gamma \left[0, \frac{aY_0^2}{2\sigma^2} \right] \right), \quad (2.22)$$

$$f_{1,\beta(1)}^{m-m}(\sigma) = -a Y_0 \beta \left(a \kappa \operatorname{Erfc} \left[Y_0 \sqrt{\frac{a}{2\sigma^2}} \right] + f_{1,\beta=0}^{m-m}(\sigma) \right), \quad (2.23)$$

$$\begin{aligned} f_{1,\beta(2)}^{m-m}(\sigma) = & a \kappa \frac{a \beta^2 \sigma^2}{2} \left\{ 2 \frac{a Y_0^2}{\sigma^2} \operatorname{Erfc} \left[Y_0 \sqrt{\frac{a}{2\sigma^2}} \right] + \right. \\ & + \frac{1}{\sqrt{\pi}} e^{-\frac{a Y_0^2}{2\sigma^2}} \left(\sqrt{\frac{a}{2\sigma^2}} Y_0 - 4 \left(\frac{a}{2\sigma^2} \right)^{3/2} Y_0^3 \right) + \\ & \left. + \frac{1}{\sqrt{\pi}} \Gamma \left[0, \frac{a Y_0^2}{2\sigma^2} \right] \left(3 \left(\frac{a}{2\sigma^2} \right)^{3/2} Y_0^3 - \sqrt{\frac{a}{2\sigma^2}} Y_0 \right) \right\}, \quad (2.24) \end{aligned}$$

where $Y_0 = \delta_c$ and $\Gamma(0, z)$ is the incomplete Gamma function. This expansion is justified by the fact that from the ellipsoidal collapse model we expect $\beta < 1$ and in [51, 52] we have shown that terms $\mathcal{O}(> \beta^3)$ are negligible²,

The collapse model affects the Gaussian mass function, $f_G(\sigma) = f_0(\sigma) + f_1(\sigma)$, in a non-trivial manner (for an exhaustive discussion we refer the reader to section III in ref. [52]). In figure 1 we plot $f_G(\sigma)$ for different values of β and D_B over the interval corresponding to the mass range probed by current NG N-body simulations ($10^{13} < M[\text{h}^{-1} M_\odot] < 10^{15}$). The spherical collapse scenario studied in [48] corresponds to $\beta = 0$ and $D_B = 0$. We can see that the effect of the average drift of the barrier (see curve with $\beta = 0.3$ and $D_B = 0$) is to suppress the mass function at all masses with respect to the spherical collapse case. Since the average threshold of collapse drifts toward larger values as function of σ , it becomes less likely for random walks to first-up crossing the barrier, thus decreasing the amplitude of $f_G(\sigma)$ more effectively in the low-mass end than at larger masses. On the other hand the effect of the stochastic diffusion (see curve with $\beta = 0$ and $D_B = 0.3$) is to facilitate the barrier crossing, thus effectively lowering the threshold of collapse. This is consistent with the presence of the factor $a = 1/(1 + D_B)$ in the exponential cut-off of the mass function, which leads

²In $f_{1,\beta(2)}^{m-m}(\sigma)$ we had previously miss a contribution. However this term is negligible for mass less than $10^{16} M_{sun}$ in [51, 52]

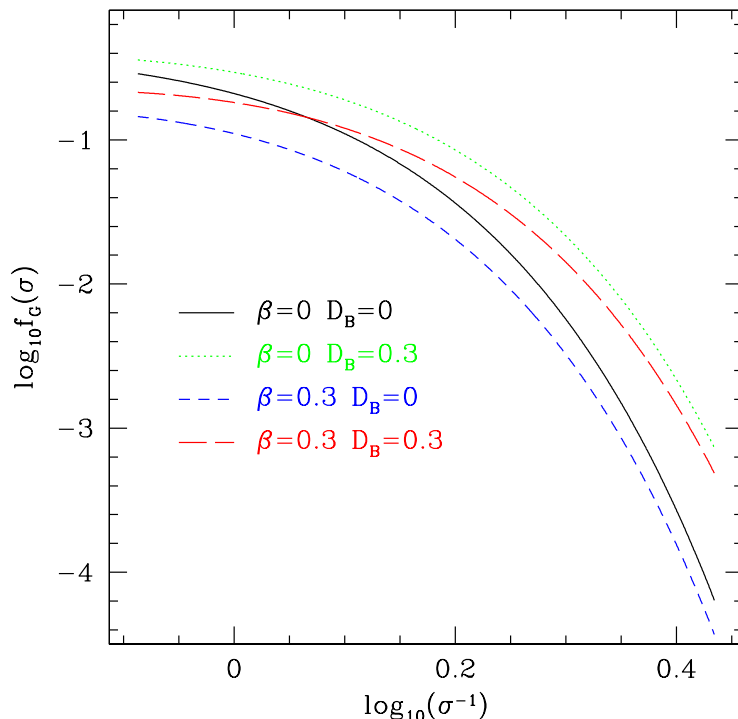


Figure 1. Gaussian excursion set halo mass function with sharp- x filter for the spherical collapse barrier (black solid line: $\beta = 0$, $D_B = 0$), a spherical diffusive barrier (green dot line: $\beta = 0$, $D_B = 0.3$), rigid moving barrier (blue short dash line: $\beta = 0.3$, $D_B = 0$) and diffusive drifting barrier (red long dash line: $\beta = 0.3$, $D_B = 0.3$).

to a larger amplitude of the mass function especially in the high-mass end. In the case of a diffusing drifting barrier (see curve with $\beta = 0.3$ and $D_B = 0.3$) these two effects compete to produce a mass function which is tilted with respect to the spherical collapse prediction.

The inclusion of the non-Markovian correction $f_1(\sigma)$ due to the filtering procedure has the effect of decreasing the amplitude of the mass function. This is because in the presence of pseudo-time correlations the random walks are characterized by smoother trajectories with less frequent jumps. This has the effect of disfavoring the first-up crossing of the barrier, thus lowering the mass function. This is consistent with the overall minus sign in eq. (2.22) and eq. (2.23) which are the leading and next-to-leading non-Markovian corrections in the mass range of interest. Here, it is also worth noticing that these expressions carry higher powers of a compared to the Markovian term $f_0(\sigma)$. This is because the effect of pseudo-time correlations on the mass function is diluted in the presence of diffusion (since diffusion always favours barrier crossing), thus leading to a faster convergence of the expansion in κ . As shown in [52], the mass function with non-Markovian corrections to first order in κ is consistent within

numerical errors with the exact numerical solution inferred from Monte Carlo generated random walks.

The study presented in [51, 52] has shown that implementing a realistic modeling of the non-spherical collapse of halos in the excursion set formalism is key to inferring a physical description of the halo mass function which is capable of reproducing results from N-body to numerical accuracy. Here, we will show that this is the case also for non-Gaussian initial conditions, since the halo collapse model directly alters the non-Gaussian signal. Previous works on the non-Gaussian halo mass function have simply reabsorbed the effects of the ellipsoidal collapse of halos in the overall Gaussian normalization function, for instance using the Sheth-Tormen formula [55]. But in doing so they have implicitly assumed that the collapse is independent of the statistics of the primordial density field and thus does not affect the non-Gaussian contribution to the halo mass function. However, we have seen that the barrier model affects both the Markovian and non-Markovian part of the halo mass function. Since non-Gaussianity appears as a non-Markovian correction to the Gaussian term, it is reasonable to expect that the stochastic barrier directly affects the dependence of the halo mass function on primordial non-Gaussianity. We will show this in detail in the next sections.

3 Non-Gaussian Halo Mass Function

In order to compute eq. (2.18) we need to first address the scale dependence of the three-point correlator of the smoothed linear non-Gaussian density field. Following [50] we expand $\langle \delta_i \delta_j \delta_k \rangle_c$ in a triple Taylor series around $S_i = S_j = S_k = S_n$ ³:

$$\langle \delta(S_i) \delta(S_j) \delta(S_k) \rangle_c = \sum_{p,q,r=0}^{\infty} \frac{(-1)^{p+q+r}}{p!q!r!} (S_n - S_i)^p (S_n - S_j)^q (S_n - S_k)^r G_3^{(p,q,r)}(S_n), \quad (3.1)$$

where

$$G_3^{(p,q,r)}(S_n) \equiv \frac{d^p}{dS_i^p} \frac{d^q}{dS_j^q} \frac{d^r}{dS_k^r} \langle \delta(S_i) \delta(S_j) \delta(S_k) \rangle_c \Big|_{S_i=S_j=S_k=S_n}. \quad (3.2)$$

In the large mass limit ($S_n \rightarrow 0$), where we expect that the primordial NG signature to be less altered by non-linear effects, the leading contribution is given by the term $\langle \delta^3(S_n) \rangle$, corresponding to $p + q + r = 0$. The next-to-leading order is given by $p + q + r = 1$ corresponding to three terms proportional to derivative of $\langle \delta(S_i) \delta^2(S_n) \rangle$ and so on, thus

$$\Pi_{NG}^\epsilon(Y_0, Y_n, S_n) = \Pi_{NG}^{\epsilon,L}(Y_0, Y_n, S_n) + \Pi_{NG}^{\epsilon,NL}(Y_0, Y_n, S_n) + \dots \quad (3.3)$$

In [57], the authors have computed the excursion set non-Gaussian mass function for a generic rigidly moving barrier modeled as a Taylor expansion in S_n up to leading order. Here, we provide an exact computation for the stochastic barrier with linearly drifting average up to next-to-leading order.

³In [56] the authors compute the path-integral through a saddle-point technique and identify scale dependent small parameters which allow them to infer a mass function which is valid over a larger range of masses.

3.1 Leading Term

The zero order term $p = q = r = 0$ reads as

$$\Pi_{NG}^{\epsilon,L}(Y_0, Y_n, S_n) = -\frac{1}{6} \langle \delta^3(S_n) \rangle \sum_{i,j,k=1}^n \int_{Y_c}^{\infty} dY_1 \dots \int_{Y_c}^{\infty} dY_{n-1} \partial_i \partial_j \partial_k W_0(Y_0, \dots, Y_n, S_n), \quad (3.4)$$

We can decompose the sum as

$$\sum_{i,j,k=1}^n \partial_i \partial_j \partial_k = \partial_n^3 + 3 \sum_{i=1}^{n-1} \partial_n^2 \partial_i + 3 \sum_{i,j=1}^{n-1} \partial_n \partial_i \partial_j + \sum_{i,j,k=1}^{n-1} \partial_i \partial_j \partial_k, \quad (3.5)$$

the integrals associated to these terms can be computed using the fact that

$$\frac{\partial}{\partial Y_c} \Pi_0^\epsilon(Y_0, Y_n, S_n) = - \sum_{i=1}^{n-1} \int_{Y_c}^{\infty} dY_1 \dots \int_{Y_c}^{\infty} dY_{n-1} \partial_i W_0(Y_0, \dots, Y_n, S_n), \quad (3.6)$$

$$\frac{\partial^2}{\partial Y_c^2} \Pi_0^\epsilon(Y_0, Y_n, S_n) = \sum_{i,j=1}^{n-1} \int_{Y_c}^{\infty} dY_1 \dots \int_{Y_c}^{\infty} dY_{n-1} \partial_i \partial_j W_0(Y_0, \dots, Y_n, S_n), \quad (3.7)$$

and

$$\frac{\partial^3}{\partial Y_c^3} \Pi_0^\epsilon(Y_0, Y_n, S_n) = - \sum_{i,j,k=1}^{n-1} \int_{Y_c}^{\infty} dY_1 \dots \int_{Y_c}^{\infty} dY_{n-1} \partial_i \partial_j \partial_k W_0(Y_0, \dots, Y_n, S_n). \quad (3.8)$$

The first-crossing distribution is given by eq. (2.8) and one can easily show that the integrals in dY_n (in the continuous limit) of the first three terms in eq. (3.5) vanish. Thus, the only non-vanishing contribution to the first-crossing distribution is given by the term in eq. (3.8) such that:⁴

$$\mathcal{F}_{NG}^L(S) = \frac{1}{6} \frac{\partial}{\partial S} \left[\langle \delta^3(S) \rangle \frac{\partial^3 I_L}{\partial Y_c^3} \Big|_0 \right], \quad (3.9)$$

where

$$I_L = \int_{Y_c}^{\infty} \Pi_0(Y_0, Y_c, Y, S) dY. \quad (3.10)$$

This integral can be computed exactly using the Markovian solution [52]

$$\Pi_0(Y_0, Y_c, Y, S) = \sqrt{\frac{a}{2\pi S}} e^{a\beta(Y-Y_0-\beta S/2)} \left[e^{-\frac{a}{2S}(Y-Y_0)^2} - e^{-\frac{a}{2S}(2Y_c-Y-Y_0)^2} \right], \quad (3.11)$$

⁴Following the same derivation it is easy to obtain the non-Gaussian contribution to the halo mass function from a non-vanishing 4-point correlation function by expanding the path-integral eq. (2.11) to first order in $\langle \delta_i \delta_j \delta_k \delta_l \rangle$. Then, to leading order in $S_i = S_j = S_k = S_l = S_n$ the first crossing distribution is $-\frac{1}{4!} \frac{\partial}{\partial S} \left[\langle \delta^4(S) \rangle \frac{\partial^4}{\partial Y_c^4} \int_{Y_c}^{\infty} dY \Pi_0(Y_0, Y, S) \right]$.

obtaining

$$I_L = \frac{1}{2} \left\{ \text{Erfc} \left(\frac{Y_c - Y_0 - \beta S}{\sqrt{2S(1 + D_B)}} \right) - e^{2\beta \frac{Y_c - Y_0}{1 + D_B}} \text{Erfc} \left(\frac{Y_0 - Y_c - \beta S}{\sqrt{2S(1 + D_B)}} \right) \right\}. \quad (3.12)$$

Substituting this expression in eq. (3.9) and using the fact that $f(\sigma) = 2\sigma^2 \mathcal{F}(\sigma)$ we finally obtain

$$\begin{aligned} f_{NG}^L(\sigma) = & \sqrt{\frac{2}{\pi}} e^{-\frac{a(Y_0 + \beta\sigma^2)^2}{2\sigma^2}} \frac{a^{3/2}\sigma}{6} \left\{ S_3(\sigma) \left[\frac{a^2}{\sigma^4} Y_0^4 - 2\frac{a}{\sigma^2} Y_0^2 - 1 + 3\frac{a^2}{\sigma^2} \beta Y_0^3 + \right. \right. \\ & + 3a\beta Y_0 + a^2\beta^3\sigma^2 Y_0 + 3a^2(\beta Y_0)^2 + 13a\beta^2\sigma^2 \left. \right] + \\ & + \frac{dS_3(\sigma)}{d\ln\sigma} \left[\frac{a}{\sigma^2} Y_0 - 1 + 3a\beta Y_0 + 4a\beta^2\sigma^2 \right] \left. \right\} + \\ & + e^{-2a\beta Y_0} \text{Erfc} \left[\sqrt{\frac{a}{2\sigma^2}} (Y_0 - \beta\sigma^2) \right] \frac{a^{3/2}\sigma}{3} 2\beta^3 (a\sigma)^{3/2} \left\{ 4S_3(\sigma) + \frac{dS_3(\sigma)}{d\ln\sigma} \right\} \end{aligned} \quad (3.13)$$

where we have introduced the reduced cumulant $\mathcal{S}_3(\sigma) = \langle \delta^3(S) \rangle / \sigma^4$. For the spherical collapse barrier, i.e. $\beta = 0$ and $a = 1$ ($D_B = 0$), the above expression reduces to Loverde et al. [43] formula as already noticed in [50]. On the other hand, it is worth noticing the presence of additional mixing terms proportional to powers of β which couple the effects of the non-spherical halo collapse to primordial non-Gaussianity.

3.2 Next-to-Leading Term

The next term in the expansion eq. (3.1) correspond to $p + q + r = 1$ (i.e. $p = 1$ and $q = r = 0$ plus permutations)

$$\Pi_{NG}^{\epsilon, NL}(Y_0, Y_n, S_n) = 3 \times \frac{1}{6} G_3^{(1,0,0)}(S_n) \sum_{i=1}^n (S_n - S_i) \sum_{j,k=1}^n \int_{Y_c}^{\infty} dY_1 \dots \int_{Y_c}^{\infty} dY_{n-1} \partial_i \partial_j \partial_k W_0, \quad (3.14)$$

where⁵

$$G_3^{(1,0,0)}(S_n) \equiv \left[\frac{d}{dS_i} \langle \delta(S_i)^2 \delta(S_n) \rangle \right]_{S_i=S_n}. \quad (3.15)$$

Again, decomposing the sum and using $\sum_{j,k=1}^{n-1} \rightarrow \partial^2 / \partial Y_c^2$, we obtain

$$\int_{Y_c}^{\infty} dY_n \Pi_{NG}^{\epsilon, NL}(Y_0, Y_n, S_n) = \frac{1}{2} G_3^{(1,0,0)}(S_n) \sum_{i=1}^n (S_n - S_i) \frac{\partial^2}{\partial Y_c^2} \left[\int_{Y_c}^{\infty} dY_1 \dots \int_{Y_c}^{\infty} dY_n \partial_i W_0 \right]. \quad (3.16)$$

⁵We have $G_3^{(1,0,0)}(S_n) = G_3^{(0,1,0)}(S_n) = G_3^{(0,0,1)}(S_n)$ since the 3-point correlation function $\langle \delta_i \delta_j \delta_k \rangle$ is symmetric under permutation of the indices, a property that results of the fact that its dependence on S_i , S_j and S_k is given by the product of three identical filter functions computed at R_i , R_j and R_k respectively.

The multiple integral in the above expression can be computed by part and using the fact that W_0 obeys the Chapman-Kolmogorov equation we can rewrite the integrand as

$$W_0(Y_0, \dots, Y_{i-1}, Y_i = Y_c, Y_{i+1}, \dots, Y_n, S_n) = W_0(Y_0, \dots, Y_c, S_i) W_0(Y_c, \dots, Y_n, S_n - S_i). \quad (3.17)$$

After taking the continuous limit, the first-crossing distribution at next-to-leading order reads as

$$\mathcal{F}_{NG}^{NL}(S) = -\frac{1}{2} \frac{\partial}{\partial S} \left[G_3^{(1,0,0)}(S) \frac{\partial^2 I_{NL}}{\partial Y_c^2} \Big|_0 \right], \quad (3.18)$$

where

$$I_{NL} = - \int_0^S dS' (S - S') \Pi_0^f(Y_0, Y_c, S') \int_{Y_c}^\infty dY \Pi_0^f(Y_c, Y, S - S'), \quad (3.19)$$

with $\Pi_0^f(Y_0, Y_c, S)$ and $\Pi_0^f(Y_c, Y, S - S')$ are the finite pseudo-time corrections at the barrier location (see [52]):

$$\Pi_0^f(Y_0, Y_c, S) = \frac{a}{\sqrt{\pi} S^{3/2}} (Y_c - Y_0) e^{-\frac{a}{2S} (Y_0 - Y_c + \beta S)^2} \quad (3.20)$$

$$\Pi_0^f(Y_c, Y, S) = \frac{a}{\sqrt{\pi} S^{3/2}} (Y - Y_c) e^{-\frac{a}{2S} (Y - Y_c - \beta S)^2}, \quad (3.21)$$

eq. (3.19) can be computed analytically using the fact that

$$\int_0^S dS_i \frac{e^{-\frac{a^2}{2S_i}} e^{-\frac{b^2}{2(S-S_i)}}}{S_i^{1/2} (S - S_i)^{3/2}} = \frac{1}{b} \sqrt{\frac{2\pi}{S}} e^{-\frac{1}{2S} (a+b)^2}, \quad (3.22)$$

we obtain

$$I_{NL} = a e^{2a\beta(Y_c - Y_0)} \text{Erfc} \left[\sqrt{\frac{a}{2\sigma^2}} (Y_0 - Y_c - \beta\sigma^2) \right] + \sqrt{\frac{2}{\pi}} \sqrt{a\sigma} e^{-a \frac{(Y_0 - Y_c + \beta\sigma^2)^2}{2\sigma^2}} \quad (3.23)$$

Introducing $\mathcal{U}_3(S) \equiv \frac{3}{S} G_3^{(1,0,0)}(S)$ we finally obtain the multiplicity function to next-leading order

$$\begin{aligned} f_{NG}^{NL}(\sigma) &= \frac{-1}{\sqrt{2\pi}} e^{-a \frac{(Y_0 + \beta\sigma^2)^2}{2\sigma^2}} \frac{a^{3/2}\sigma}{3} \\ &\left\{ U_3(\sigma) \left[1 + \frac{a}{\sigma^2} Y_0^2 + 15a\beta^2\sigma^2 + 4a\beta Y_0 \right] + \frac{dU_3(\sigma)}{d \ln \sigma} \left[1 + 4a\beta^2\sigma^2 \right] \right\} - \\ &- e^{-2a\beta Y_0} \text{Erfc} \left[\sqrt{\frac{a}{2\sigma^2}} (Y_0 - \beta\sigma^2) \right] \frac{a^{3/2}\sigma}{3} \\ &\left\{ U_3(\sigma) \left[4\sqrt{a}\beta\sigma + 8(a)^{3/2}(\beta\sigma)^3 - 4a^{3/2}\beta^2\sigma Y_0 \right] + \right. \\ &\left. + \frac{dU_3(\sigma)}{d \ln \sigma} \left[2\sqrt{a}\beta\sigma + 2a^{3/2}(\beta\sigma)^3 - 2a^{3/2}\beta^2\sigma Y_0 \right] \right\} \end{aligned} \quad (3.24)$$

As in the case of the leading order term we notice the presence of additional mixing terms in powers of β . This clearly indicates that contrary to standard derivations of the NG mass function based on the Press-Schechter formalism, the effect of the non-spherical collapse of halos cannot be simply reabsorbed in the Gaussian part of the mass function, but directly alters the non-Gaussian dependence⁶.

4 Local and Equilateral Non-Gaussian Mass Function

4.1 Reduced bispectra and fitting functions

In deriving the non-Gaussian terms we have made no assumptions on the specific type of non-Gaussianity. In the case of non-Gaussianity with non-vanishing skewness the three-point correlation function of the smoothed linear density field at $z = 0$ formally reads as:

$$\begin{aligned} \langle \delta(R_1)\delta(R_2)\delta(R_3) \rangle_c &= \int \frac{d^3k_1}{(2\pi)^3} \int \frac{d^3k_2}{(2\pi)^3} \int \frac{d^3k_3}{(2\pi)^3} \tilde{W}(k_1, R_1) \tilde{W}(k_2, R_2) \tilde{W}(k_3, R_3) \times \\ &\times \mathcal{M}(k_1)\mathcal{M}(k_2)\mathcal{M}(k_3) \langle \zeta(\mathbf{k}_1)\zeta(\mathbf{k}_2)\zeta(\mathbf{k}_3) \rangle_c, \end{aligned} \quad (4.1)$$

where

$$\mathcal{M}(k) = \frac{2}{5H_0^2\Omega_m} T(k)k^2, \quad (4.2)$$

with H_0 being the Hubble constant, Ω_m the matter density relative to the critical one, $T(k)$ the transfer function at $z = 0$ and $\zeta(k)$ is the curvature perturbation with

$$\langle \zeta(\mathbf{k}_1)\zeta(\mathbf{k}_2)\zeta(\mathbf{k}_3) \rangle_c = (2\pi)^3 \delta_D(\mathbf{k}_1 + \mathbf{k}_2 + \mathbf{k}_3) B_\zeta(k_1, k_2, k_3), \quad (4.3)$$

where $B_\zeta(k_1, k_2, k_3)$ is the reduced bispectrum and encodes the characteristic momentum dependence of the non-Gaussian signal. The dependence on the Dirac- δ function, $\delta_D(\mathbf{k})$, ensures the momentum conservation, implying that admitted momentum space configurations form closed triangles.

A variety of models, including standard inflation, predicts

$$B_\zeta(k_1, k_2, k_3) = \frac{6}{5} f_{NL}^{\text{loc}} [P_\zeta(k_1)P_\zeta(k_2) + P_\zeta(k_1)P_\zeta(k_3) + P_\zeta(k_2)P_\zeta(k_3)], \quad (4.4)$$

where f_{NL}^{loc} is a constant amplitude and $P_\zeta(k) = A_s k^{n_s-4}$ is the primordial power spectrum. This type of non-Gaussianity is also known as ‘‘local’’ since the curvature perturbation at any point in space can be written in terms of a linear Gaussian field, $\zeta_G(\mathbf{x})$:

$$\zeta(\mathbf{x}) = \zeta_G(\mathbf{x}) + \frac{3}{5} f_{NG}^{\text{loc}} [\zeta_G^2(\mathbf{x}) - \langle \zeta_G^2(\mathbf{x}) \rangle]. \quad (4.5)$$

⁶Notice that the non-Gaussian terms for $\beta = 0$ do not exactly coincide with the corresponding formulae in [50] neglecting the mixing terms in $a\kappa$ and f_{NL} . The mass function for a diffusive stochastic barrier cannot be inferred from the spherical collapse scale by a simple rescaling of the variables including the skewness of the initial density field.

In such a case the non-Gaussian signal peaks around momentum space configurations for which one of the momenta is much smaller than the others (e.g. $k_1 \ll k_2 \approx k_3$). WMAP-7yr measurements of the CMB bispectrum constrain the amplitude of local non-Gaussianity in the range $-10 < f_{NL}^{\text{loc}} < 74$ at 2σ [58].

Alternatively, models in which primordial density fluctuations are generated by a field subject to higher-derivative terms predict a reduced bispectrum of the form

$$B_\zeta(k_1, k_2, k_3) = \frac{18}{5} f_{NL}^{\text{equi}} A_s^2 \left[\frac{1}{2k_1^{4-n_s} k_2^{4-n_s}} + \frac{1}{3(k_1 k_2 k_3)^{2(4-n_s)/3}} + \frac{1}{(k_1 k_2^2 k_3^3)^{(4-n_s)/3}} + 5 \text{ perm.} \right]. \quad (4.6)$$

This is also known as ‘‘equilateral’’ non-Gaussianity, since the signal maximizes in momentum space configurations for which $k_1 \approx k_2 \approx k_3$. WMAP-7yr measurements constrain the amplitude of equilateral non-Gaussianity in the range $-214 < f_{NL}^{\text{equi}} < 266$ at 2σ [58].

We integrate eq. (4.1) numerically for local and equilateral type of non-Gaussianities and infer \mathcal{S}_3 , $d\mathcal{S}_3/d\ln\sigma$, \mathcal{U}_3 and $d\mathcal{U}_3/d\ln\sigma$. The transfer function has been computed for a vanilla Λ CDM model best fit to WMAP-5 years data using the CMBFAST code [59]. The functions are plot in figure 2 and 3 respectively, over the mass range probed by current non-Gaussian N-body simulations (e.g., see refs. [37, 38]), which corresponds to $-0.1 \lesssim \log_{10}(1/\sigma) \lesssim 0.5$. As shown in the bottom panels these functions can be approximated to better than a few percent accuracy by simple fitting formulae. In the local case we find

$$\mathcal{S}_3^{\text{loc}}(\sigma) = f_{NL}^{\text{loc}} 10^{-4} \left[1.54882 \left(\frac{1}{\sigma} \right)^{0.81} \right] \quad (4.7)$$

$$\frac{d\mathcal{S}_3^{\text{loc}}}{d\ln\sigma} = f_{NL}^{\text{loc}} 10^{-3} \left[2.24881 e^{-0.421266 \ln^2(\frac{1}{\sigma})} \left(\frac{1}{\sigma} \right)^{2.6856} \right] \quad (4.8)$$

$$\mathcal{U}_3^{\text{loc}}(\sigma) = f_{NL}^{\text{loc}} 10^{-4} \left[-1.78409 + 1.67796 \ln \left(\frac{1}{\sigma} \right) - 0.471529 \ln^2 \left(\frac{1}{\sigma} \right) \right] \quad (4.9)$$

$$\frac{d\mathcal{U}_3^{\text{loc}}}{d\ln\sigma} = f_{NL}^{\text{loc}} 10^{-3} \left[-4.20811 - 5.7224 \ln \left(\frac{1}{\sigma} \right) + 8.88 \ln^2 \left(\frac{1}{\sigma} \right) \right], \quad (4.10)$$

while for equilateral NG we have

$$\mathcal{S}_3^{\text{equi}}(\sigma) = f_{NL}^{\text{equi}} 10^{-4} \left[0.301995 \left(\frac{1}{\sigma} \right)^{0.86} \right] \quad (4.11)$$

$$\frac{d\mathcal{S}_3^{\text{equi}}}{d\ln\sigma} = f_{NL}^{\text{equi}} 10^{-3} \left[1.56939 e^{-0.399551 \ln^2(\frac{1}{\sigma})} \left(\frac{1}{\sigma} \right)^{2.7182} \right] \quad (4.12)$$

$$\mathcal{U}_3^{\text{equi}}(\sigma) = f_{NL}^{\text{equi}} 10^{-4} \left[0.33 - 1.52675 \left(\frac{1}{\sigma} \right)^{0.694871} \right] \quad (4.13)$$

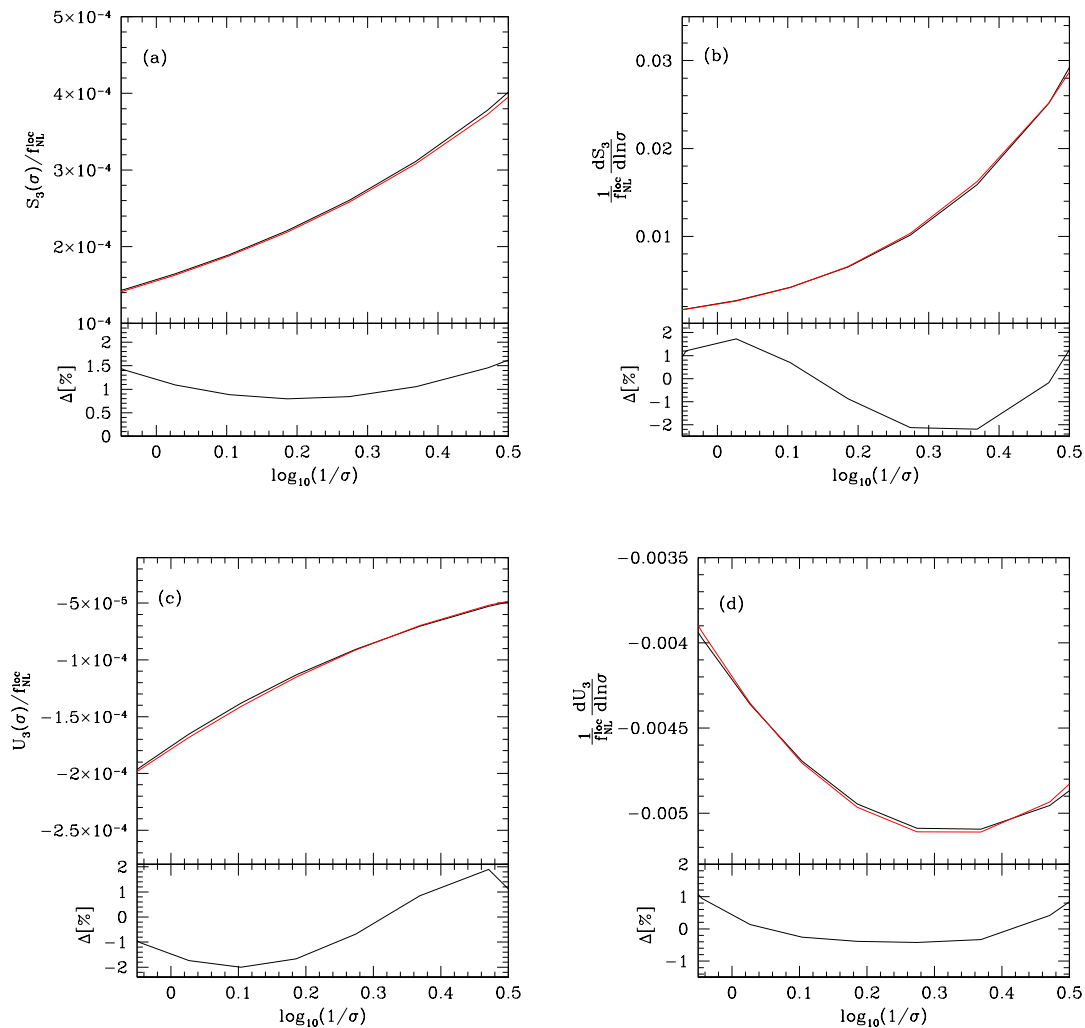


Figure 2. \mathcal{S}_3 (a), $d\mathcal{S}_3/d\ln\sigma$ (b), \mathcal{U}_3 (c) and $d\mathcal{U}_3/d\ln\sigma$ (d) for local non-Gaussianity. Black solid curves are the numerically computed functions obtained from numerical integration of eq. (4.1). Red solid curves correspond to fitting formulae eqs. (4.7)-(4.10) with a few percent errors (bottom panels).

$$\frac{d\mathcal{U}_3^{\text{equi}}}{d\ln\sigma} = f_{NL}^{\text{equi}} 10^{-3} \left[1.21732 - 0.489189 \ln\left(\frac{1}{\sigma}\right) + 0.26217 \ln^2\left(\frac{1}{\sigma}\right) \right]. \quad (4.14)$$

4.2 Validity of the perturbative expansions

We have inferred the halo mass function in the presence of primordial non-Gaussianity as an expansion about the Gaussian Markovian solution by Taylor expanding the path-integral eq. (2.13) to first order in the three-point correlation function. Furthermore, we have expanded this correlator as a triple series in powers of the variance S which we have truncated to the next-to-leading order to obtain $f_{NG}(\sigma) = f_{NG}^L(\sigma) + f_{NG}^{NL}(\sigma)$. In this section we derive limits on the mass range and the amplitude of the skewness

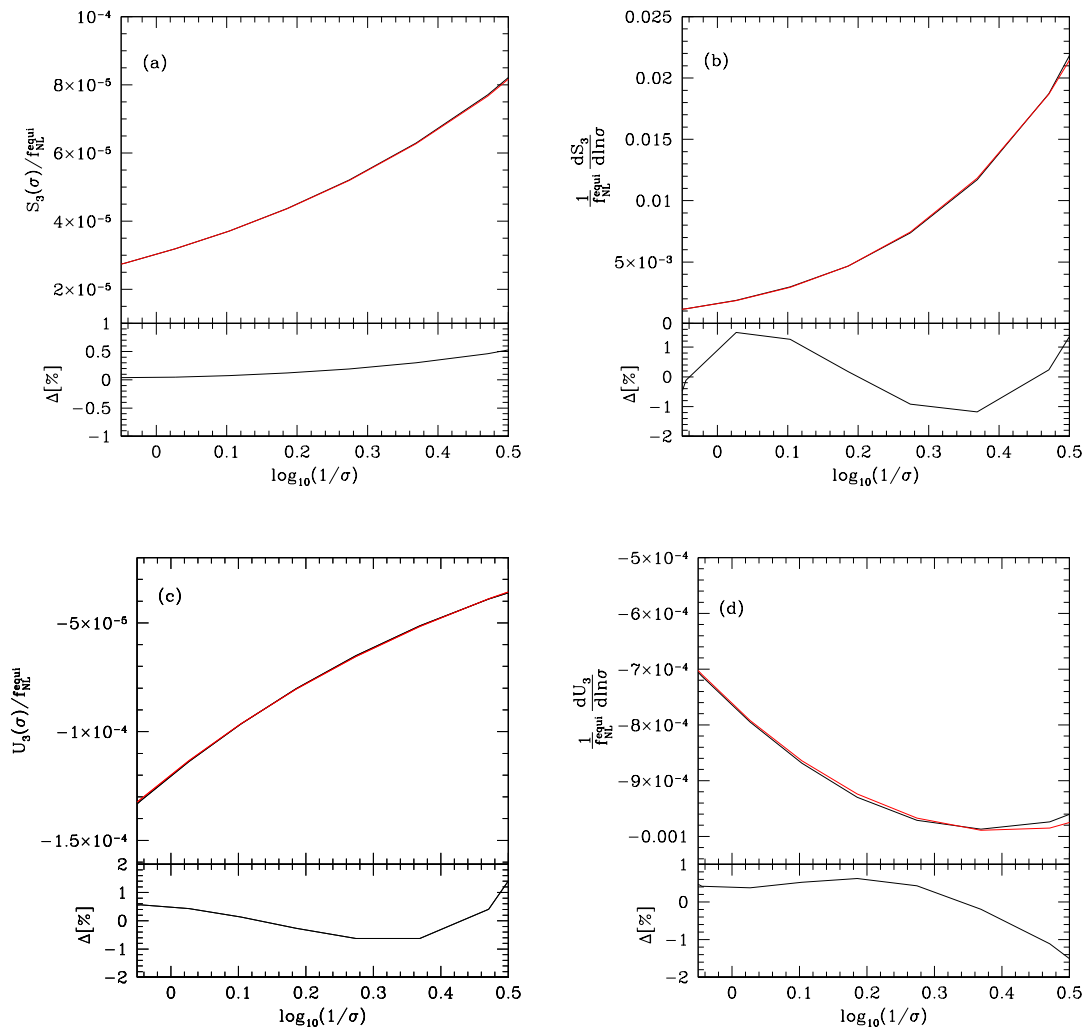


Figure 3. As in figure 2 for equilateral non-Gaussianity. Fitting formulae are given by eqs. (4.11)-(4.14)

parameter that bound the validity of such a perturbative approach.

4.2.1 Limits on the mass range

In order to infer the range of validity of the expansion of $\langle \delta(S)\delta(S')\delta(S'') \rangle$ in power of S up to next-to-leading order let us consider the ratio $r_{NL-L} = f_{NL}^{NL}(\sigma)/f_{NL}^L(\sigma)$. Independently of the value of f_{NL} the perturbative expansion breaks down for values of σ such that $r_{NL-L} > 1$. In such a case the exact functional form of $\langle \delta(S)\delta(S')\delta(S'') \rangle$ must be taken into account.

In figure 4 we plot $\log_{10} |r_{NL-L}|$ for local (left panel) and equilateral (right panel) non-Gaussianities and different barrier parameter values corresponding to different collapse scenarios. In both cases we notice that $|r_{NL-L}| \ll 1$ in the high-mass end (i.e. large values $\log_{10} \sigma^{-1}$), while $r_{NL-L} \rightarrow 1$ in the small-mass end. This is expected since

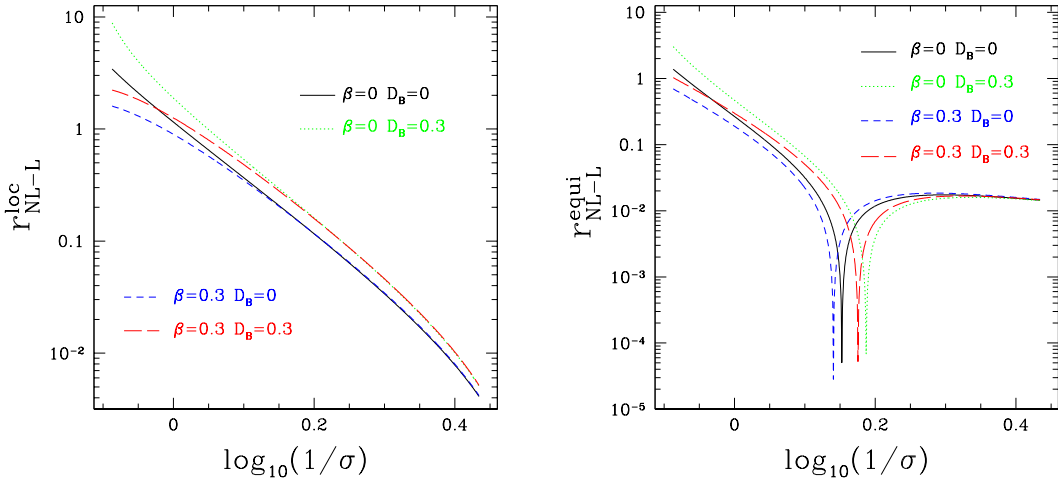


Figure 4. r_{NL-L} as function of $\log_{10} \sigma^{-1}$ for local (left panel) and equilateral (right panel) non-Gaussianities. Different curves correspond to the spherical collapse barrier (black solid line), a spherical diffusive barrier (green dot line), rigid moving barrier (blue short dash line) and diffusive drifting barrier (red long dash line) as shown in fig. 1.

eq. (3.1) is a good approximation of the three-point correlation function in the large scale limit ($S \rightarrow 0$). On the other hand, higher-derivative corrections in S become relevant at smaller scales, until the expansion eventually breaks down. The exact scale at which this occurs depends on the halo collapse model parameters. For local NG we have $r_{NL-L} > 1$ at $\log_{10} \sigma^{-1} < 0.01$ in the spherical collapse case (black solid line), $\log_{10} \sigma^{-1} < 0.05$ for a spherical diffusive barrier (green dot line), $\log_{10} \sigma^{-1} < -0.01$ for a rigid moving barrier (short dash blue line) and $\log_{10} \sigma^{-1} < 0.03$ for a diffusive drifting barrier (red long dash line). Such differences are a direct manifestation of the model collapse imprints on the non-Gaussian contribution to the halo mass function. In particular, we may notice that the barrier diffusion systematically increases the value of r_{NL-L} , thus reducing the range of validity of the perturbative expansion. In contrast, the average drift of the barrier has the opposite effect of diminishing the value of r_{NL-L} as function of σ . In the equilateral case we observe a similar trend with two distinctive features. First, $|r_{NL-L}| < 1$ over a wider mass range than in the local case. Moreover the ratio exceeds unity only in the case of the spherical barrier ($\beta = 0$ and $D_B = 0$) for $\log_{10} \sigma^{-1} > -0.07$ and the diffusive spherical barrier ($\beta = 0$ and $D_B = 0.3$) for $\log_{10} \sigma^{-1} > -0.04$. Second, depending on the collapse model the ratio flips sign at $\log_{10} \sigma^{-1} \approx 0.1$, due to the fact that for equilateral NG the term $f_{NG}^{NL}(\sigma)$ is negative in the small-mass end and increases towards positive values in the high-mass end, while $f_{NG}^L(\sigma)$ is always positive.

4.2.2 Limits on f_{NL}

Having established the mass range of validity of $f_{NG}(\sigma)$ we can now infer an upper limit on f_{NL} by imposing the ratio $|f_{NG}(\sigma)/f_0(\sigma)| < 1$.

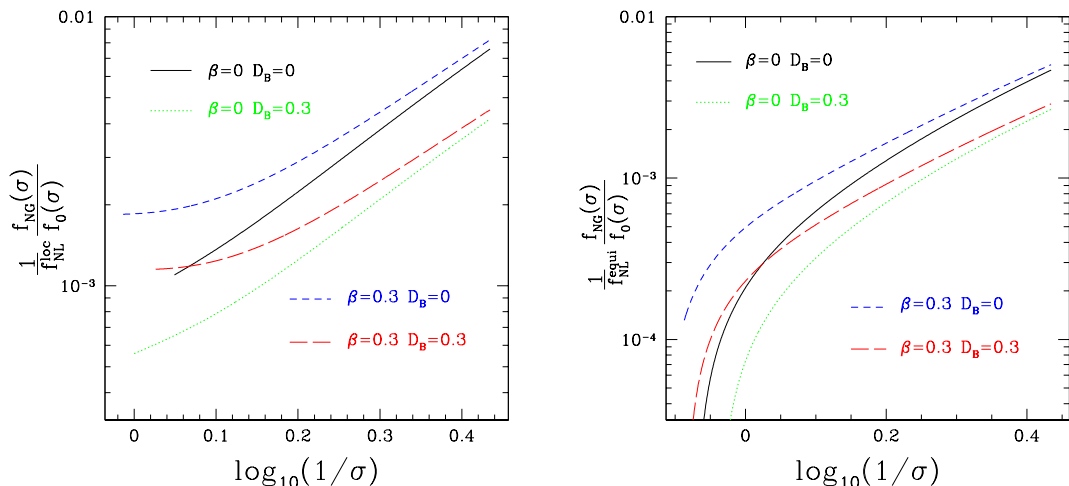


Figure 5. r_{NG-G} as function of $\log_{10} \sigma^{-1}$ for local (left panel) and equilateral (right panel) non-Gaussianities in units of f_{NL} . Different curves correspond to the collapse models shown in fig. 1.

In figure 5 we plot $f_{NG}(\sigma)/f_0(\sigma)$ for local (left panel) and equilateral (right panel) non-Gaussianities in units of f_{NL} over the range of validity of eq. (3.1) for the barrier model parameters shown in figure 1. First, we may notice that in the local case the ratio increases toward large value of $\log_{10} \sigma^{-1}$ and maximizes in the high-mass end. Secondly, the overall amplitude of this ratio varies for different barrier model parameter values. This is an indication that the non-Gaussian imprint on the halo mass function depends on the collapse model which we will discuss in more detail in the next section. A similar trend occurs in the equilateral case, the main difference result in the low-mass behavior and the value of the ratio in the high-mass end. From these curves we infer that the ratio becomes of order of unity in the high-mass end for $|f_{NL}^{loc}| \approx 200$ and $|f_{NL}^{equi}| \approx 500$ respectively in the diffusive drifting barrier with $\beta = 0.3$ and $D_B = 0.3$. Similar upper limits correspond to the barrier model with $\beta = 0$ and $D_B = 0.3$, while for rigid barriers with $D_B = 0$ these upper limits are nearly a factor of two smaller. Nevertheless, these values are much larger than current WMAP bounds. Therefore, the mass function derived here can be used for observational analysis purposes to test primordial NG on masses $M > 2 \cdot 10^{10} h^{-1} M_{\odot}$ for realistic values of f_{NL} .

5 Halo Collapse Model and NG Signal

We now discuss the imprints of primordial non-Gaussianity on the halo mass function and the dependence on the halo collapse model parameters. In order to evaluate the NG features it has become standard to consider the ratio $\mathcal{R} = f(\sigma)/f_G(\sigma)$, which we plot in figure 6 for local NG (left panel) and equilateral NG (right panel) for $f_{NL} = -50, -20, 20$ and 50 , in the range of validity of $f(\sigma)$ for the barrier model parameter values shown in figure 1. We can see that the independently of the value

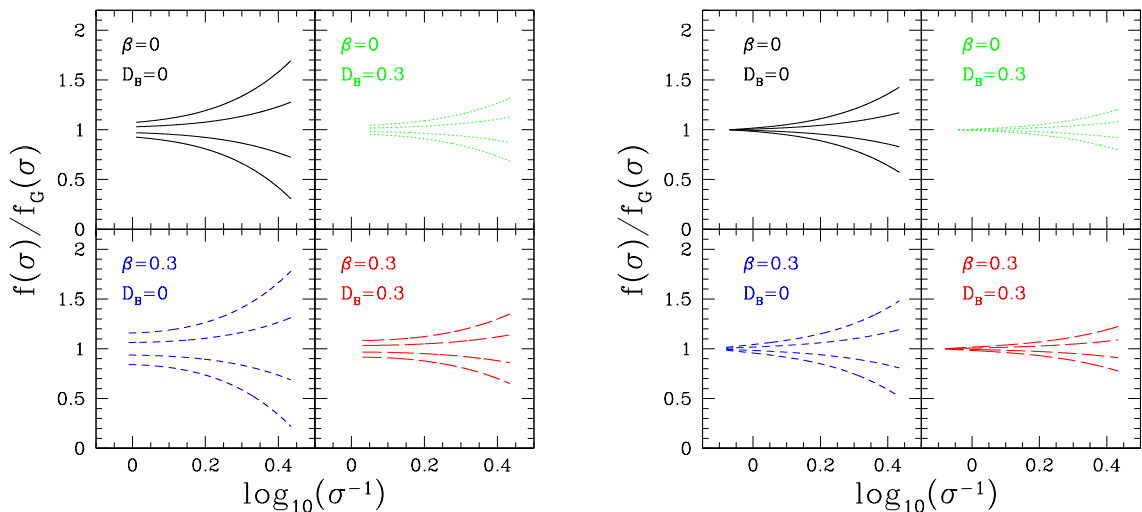


Figure 6. $\mathcal{R} = f(\sigma)/f_G(\sigma)$ as function of $\log_{10} \sigma^{-1}$ for local (left panel) and equilateral (right panel) non-Gaussianities with $f_{NL} = -50, -20, 20$ and 50 (curves from bottom to top) and different barrier parameter values.

of β and D_B the deviation from the Gaussian case maximizes in the high-mass end consistently with expectations that NG affects primarily the large masses both in the local and equilateral case. However, we also notice that the non-Gaussian signature depends on the barrier model parameter values. In particular, by comparing curves with the same value of f_{NL} and different values of β and D_B we can infer two distinctive trends. On the one hand the barrier diffusion diminishes the overall amplitude of the non-Gaussian signal relative to the Gaussian one, particularly in the high-mass end. On the other hand, the average drift of the barrier enhances the NG imprint, especially at small masses. As an example in the local case with $f_{NL} = 50$ and $\beta = D_B = 0$ we find $\mathcal{R} = 1.7$ in the high-mass end, while for a spherical diffusive barrier with $\beta = 0$ and $D_B = 0.3$ we have a smaller ratio $\mathcal{R} = 1.4$. In contrast, in the small-mass end we have $\mathcal{R} = 1.1$ for the spherical case and $\mathcal{R} = 1.2$ for $\beta = 0.3$ and $D_B = 0$. Similar trends occur in the equilateral case.

As already inferred from the form of the non-Gaussian terms in section 3, this shows that the effects of statistics of the primordial matter density field and the non-spherical collapse of halos are coupled. Furthermore the nature of the imprints is consistent with the excursion set picture. In fact, primordial non-Gaussianity manifests as an additional non-Markovian correlation to the random walk trajectories. The barrier diffusion increases the likelihood of first-up crossing, while the average drift reduces it and as discussed in section 2.4, the former has the effects of diminishing the amplitude of the non-Markovian term relative to the Markovian one, while the latter enhances it.

The fact that the non-Gaussian signal depends on the halo collapse is particularly important from an observational point of view. In fact, if f_{NL} is sufficiently large

neglecting the non-spherical collapse model dependence may lead to biased results. It is plausible that such degeneracies may be broken including measurements of the redshift evolution the halo mass function. Although, this will require predicting the redshift and cosmology of the barrier model parameters for non-Gaussian initial conditions, a study which goes beyond the scope of this paper.

6 NG Halo Mass Function and N-body Simulations

In recent years, several groups have performed numerical N-body simulations with non-Gaussian initial conditions to probe the imprints of primordial non-Gaussianity on the distribution of dark matter halos [36–39]. These studies have provided fitting functions for the non-Gaussian halo mass function and tested the validity of analytical formula based on the Press-Schechter formalism. Here, we confront the mass function derived in the previous sections against the results of Pillepich, Porciani and Hahn [38]. These authors have performed a series of high-resolution runs with 1024^3 particles in large volume boxes resolving halos with mass $10^{13} < M[h^{-1}M_{\odot}] < 10^{15}$ for local NG initial conditions in the case of WMAP-3yr and WMAP5-yr calibrated cosmologies. Halo mass functions have been measured using the Friend-of-Friend algorithm with linking length $b = 0.2$ at different redshifts and fitted with the standard parametrization

$$f_{\text{fit}}(\sigma) = \left[D + B \left(\frac{1}{\sigma} \right)^A \right] e^{-\frac{C}{\sigma^2}}, \quad (6.1)$$

in doing so the authors have inferred polynomial fits which parameterize the dependence on f_{NL} and z of the coefficients A, B, C and D. Here, we limit our theoretical model comparison with the results at $z = 0$.

Before discussing the results of this comparison let us make a few remarks. The excursion set mass function for the diffusive barrier model depends on two input parameters which specifies the statistical properties of the stochastic barrier. Other quantities such as the spherical collapse threshold δ_c and the amplitude of the filter-correction κ are predicted for a given cosmological model. For instance in Λ CDM WMAP5-yr cosmology $\delta_c = 1.673$ at $z = 0$ and $\kappa = 0.475$.

In principle, the values of β and D_B can be predicted for a given cosmology. As already stressed in section 2.2 this requires estimating the properties of the stochastic barrier by numerically solving the ellipsoidal collapse model equations. As shown by Doroshkevich [60], the randomness of the initial density field causes the parameters describing a homogeneous ellipsoid to be random variable themselves with a characteristic probability distribution. By generalizing this to non-Gaussian initial conditions and solving the ellipsoidal collapse model equations one can infer the probability distribution of the collapse threshold as function of the variance of the linear density field. Then, the stochastic barrier model parameters can be derived by matching their value to the moments of the probability distribution. Such an inference will provide a complete prediction of the cosmology, redshift and non-Gaussian dependence of β and D_B which at moment is missing. However, testing such dependences against numerically inferred N-body halo mass functions will first require addressing the effect of

the second order cloud-in-cloud problem, which as we have mentioned in Section 2.2 manifests as an additional scatter on the halo collapse threshold.

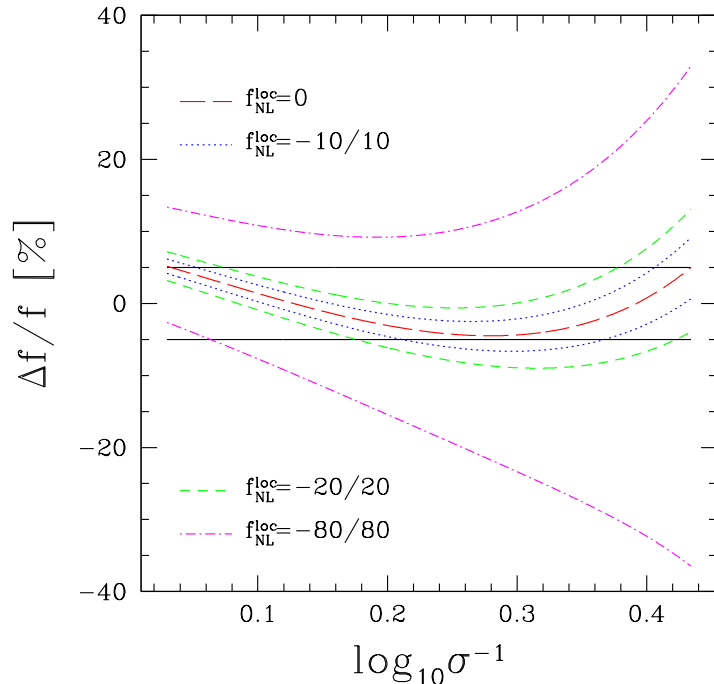


Figure 7. Relative difference of the NG mass function with respect to Pillepich et al. fitting formula for the Gaussian calibrated barrier model parameters. The discrepancy remains within the numerical accuracy of the N-body results (solid parallel lines) for $-10 \lesssim f_{NL} \lesssim 30$.

In the absence of theoretical prediction for the values of β and D_B , the diffusive drifting barrier model remains an effective description of the non-spherical collapse of halos. Consequently, the model parameters can be determined only through comparison with N-body simulation results. For instance, in [51, 52] we have confronted the Gaussian mass function N-body simulation data by Tinker et al. [63] obtained using the Spherical Overdensity (SO) algorithm. This has allowed us to infer the best fit values $\beta_G^{SO} = 0.057$ and $D_B^{SO} = 0.294$ and quite remarkably found that for such parameter values the mass function reproduces the data to numerical accuracy ($\sim 5\%$). However, we cannot assume these values to confront with the results from the Pillepich et al. simulations even for $f_{NL} = 0$. This is because there is roughly a $\sim 10\%$ scatter between SO and FoF mass functions due to systematic differences of the halo detection algorithms. Therefore we have calibrated the value of β and D_B against the Gaussian mass function from [38]. We find $\beta^G = 0.0113$ and $D_B^G = 0.3262$. Assuming such values we plot in figure 7 the relative difference between eq. (2.19) and eq. (6.1) for different values of f_{NL} . We can see that for $f_{NL} = 0$ the differences are well within the numerical uncertainties $\approx 5\%$, which is consistent with the results of the comparison to Tinker et al. [63] presented in [51, 52]. As it can be seen in figure 7,

for $f_{NL}^{\text{loc}} \neq 0$ the relative difference remains within the numerical errors only in the range $-10 \lesssim f_{NL} \lesssim 30$, while for larger values the mass function evaluated using the Gaussian calibrated parameters largely deviates from the numerical fit.

This simply implies that for f_{NL} outside this range the non-spherical collapse of halos strongly differ from the Gaussian case and consequently we can expect β and D_B to vary with f_{NL} .

We can see this more clearly by inferring the best fit values of β and D_B for different values of f_{NL} in the range $-80 < f_{NL} < 80$ for which we compare equation (2.19) against eq. (6.1) with equation (11) and table 6 in Pillepich et al. [38] with 5% accuracy; and for $80 < f_{NL} < 200$ using their parameterization equation (7) and table 4 with 10% accuracy. We plot the ratio of the best fit parameters to their Gaussian value in figure 8. We may notice that $\beta^{\text{fit}}/\beta^G$ increases for increasing values of $f_{NL} > 0$, while D_B^{fit}/D_B^G decreases.

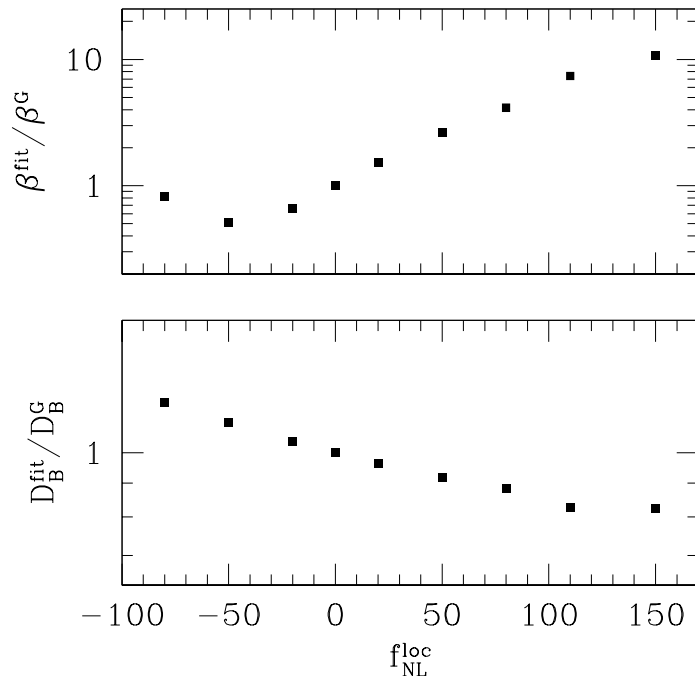


Figure 8. Best fit values of β (top panel) and D_B (bottom panel) relative to the Gaussian case as function of f_{NL} .

In particular, for large positive values of f_{NL} the average drift is about 10 times larger than in the Gaussian case. This indicates that for large primordial non-Gaussianity the collapse of dark matter halos is highly non-spherical. Furthermore, since the drifting term increases halos with higher mass will be privileged. On the other hand, the diffusion decreases with respect to the Gaussian case for increasing values of f_{NL} . Reminding that the barrier has a Gaussian distribution of mean value $\bar{B} = \delta_c + \beta S$

and variance D_B then, for positive value of f_{NL} , the non-Gaussian nature of the initial density field tends to localize the barrier around \bar{B} .

It would be interesting to perform a study similar to that of Robertson et al. [64] to infer the distribution of the linear collapse threshold of halos detected in non-Gaussian simulations, which can provide a direct confirmation of the trend of β and D_B as function of f_{NL} obtained here.

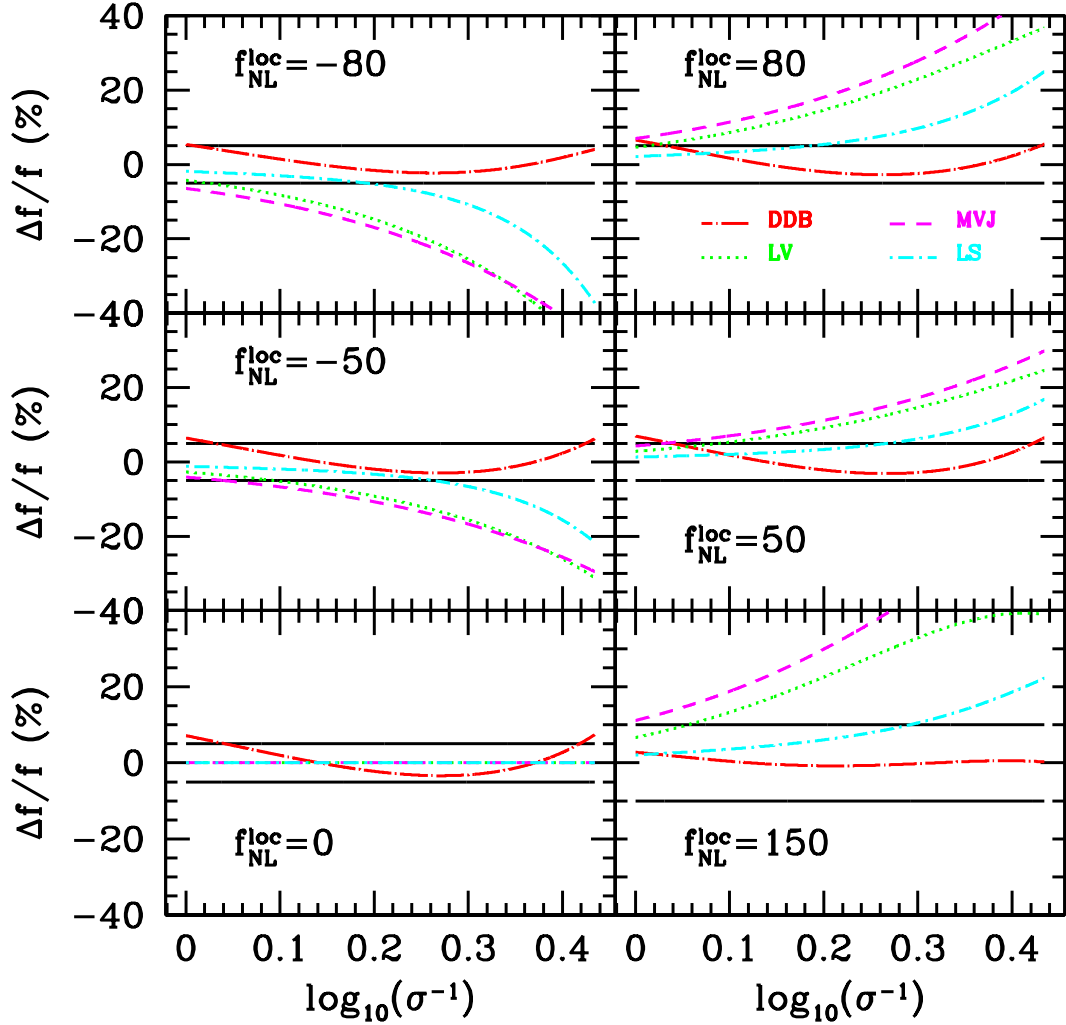


Figure 9. Relative difference with respect to the Pillepich et al. fitting formulae for different values of f_{NL}^{loc} of non-Gaussian halo mass functions for the DDB case with best fitting barrier parameter values (red long-dash dot line), Loverde et al. [43] (green dot line), Matarrese-Jimenez-Verde [42] (magenta short-dash line) and Lam-Sheth [44] (cyan short-dash dot line) respectively.

In figure 9 we show the relative difference with respect to Pillepich et al. fitting formula of the NG mass function computed with the best fit barrier parameters (red long-dash dot line) for the values of f_{NL}^{loc} used in figure 8. We can see that the differences remains within the numerical accuracy of the N-body results. In addition, we show the relative difference for the Loverde et al. [43] formula (LV, green dot line), Matarese-Verde-Jimmenez [42] (MVJ, magenta short-dash line) and Lam-Sheth [44] (LS, cyan short-dash dot line). Since the Gaussian limit of these different formulae is given by the Press-Schechter mass function, for a comparison with the N-body simulation results we have renormalized them to the Gaussian fitting formula by Pillepich et al. [38]. We find these formulae to be within the numerical accuracy of the N-body results only for small departure from Gaussianity, $f_{NL}^{loc} < 20$, for which the effects due to the non-Gaussian dependence of the non-spherical collapse is negligible. In the light of our analysis the non-spherical nature of the halo collapse must be taken into account when testing primordial non-Gaussianity with halo mass function measurements.

7 Conclusion

In the upcoming years several observational program will provide precise measurements of the number counts and spatial distribution of galaxy clusters. These measurements will provide new insights on the mass distribution of dark matter halos and consequently on the underlying cosmology and the statistics of the primordial density field.

Here, we have performed an *ab initio* calculation of the NG halo mass function using the path-integral formulation of the excursion set formalism. We have considered a stochastic model of the halo collapse threshold which captures the main features of the non-spherical collapse of halos. We have specifically focused on primordial NG due to a non-vanishing skewness of the initial density field and inferred the mass function through a perturbative expansion of the path-integral. The computation can be extended to higher-order correlations and we have showed that the effect of a non-vanishing kurtosis can be easily obtained at leading order.

Contrary to standard approaches based on NG extension of the Press-Schechter calculation, we find that the effects of the non-spherical nature of the collapse of halos on the mass function directly couples to the signature of primordial non-Gaussianity. As such, these effects cannot be simply reabsorbed in a Gaussian normalization term. We have studied the case for local and equilateral non-Gaussianities, though the formulae provided here can be applied to any NG shape function.

We have compared the inferred mass function with NG local N-body simulations results and found a remarkable agreement. Using the barrier model parameters calibrated on the Gaussian N-body mass function we find that for large non-Gaussianity ($f_{NL} < -10$ and $f_{NL} > 30$) the non-spherical collapse largely deviates from the Gaussian case and its effect cannot be simply reabsorbed in a Gaussian normalization as in the case of PS derived mass functions. These effects can, therefore, be important for cluster count studies since the non-Gaussian dependence of the non-spherical collapse of halos changes the imprint of primordial non-gaussianity on the mass function. For instance in [65] the author has shown that the abundance of clusters which do not be-

long to the superclusters, detected in Gaussian N-body simulations, is well described by the Gaussian mass function derived in [51, 52] for $D_B = 0$ and a non-vanishing β . In light of this result we can expect that the number counts of this type of clusters may be more sensitive to the signature of primordial NG since the imprint has a larger amplitude compared to field clusters with $D_B \neq 0$ and $\beta = 0$.

These results suggest several directions of future investigation. On the theoretical side it appears evident that a theoretical prediction of β and D_B based on a detailed study of the ellipsoidal collapse model is needed. This will allow us to predict the cosmology and redshift dependence as well as their relation with respect to statistics of the primordial density field. Thus, a barrier model parameter inference using mass function measurements may provide a way of distinguishing between different cosmological scenarios assuming a proper treatment of the second order cloud-in-cloud problem. On the numerical side it will be interesting to confront these model predictions with the linearly extrapolated collapse threshold of halos detected in N-body simulations for different cosmological scenarios.

Acknowledgments

We thank Ravi Sheth and Tommaso Giannantonio for his useful discussions and comments. Research for this work is supported in part by a grant of the University Paris Diderot.

References

- [1] A. H. Guth and S. Y. Pi, *Fluctuations in the new inflationary universe*, Phys. Rev. Lett. **49** (1982) 1100.
- [2] A. A. Starobinsky, *Dynamics of phase transition in the new inflationary universe and generation of perturbations*, Phys. Lett. B **117** (1982) 175.
- [3] J. M. Bardeen, P. J. Steinhardt and M. S. Turner, *Spontaneous creation of almost scale-free density perturbations in an inflationary universe*, Phys. Rev. D **28** (1983) 679.
- [4] T. Falk, R. Rangarajan and M. Srednicki, *The angular dependence of the three point correlation function of the cosmic microwave background radiation as predicted by inflationary cosmologies*, Astrophys. J. **403** (1993) L1.
- [5] A. Gangui, F. Lucchin, S. Matarrese and S. Mollerach, *The three point correlation function of the cosmic microwave background in inflationary models*, Astrophys. J. **430** (1994) 447.
- [6] V. Acquaviva, N. Bartolo, S. Matarrese and T. Riotto, *Second-order cosmological perturbations from inflation*, Nucl. Phys. B **667** (2003) 119.
- [7] J. M. Maldacena, *Non-Gaussian features of primordial fluctuations in single field inflationary models*, J. High Energy Phys. JHEP05(2003)013.
- [8] N. Arkani-Hamed, P. Creminelli, S. Mukohyama and M. Zaldarriaga, *Ghost inflation*, JCAP04(2004)001.

- [9] D. H. Lyth, C. Ungarelli and D. Wands, *The primordial density perturbation in the curvaton scenario*, Phys. Rev. D **67** (2003) 023503.
- [10] P. Creminelli, *On non-Gaussianities in single-field inflation*, JCAP 10(2003)003.
- [11] M. Alishahiha, E. Silverstein and D. Tong, *DBI in the sky*, Phys. Rev. D **70** (2004) 123505.
- [12] L. Senatore, *Tilted ghost inflation*, Phys. Rev. D **71** (2005) 043512.
- [13] X. Chen, R. Easther and E. A. Lim, *Large non-Gaussianities in single field inflation*, JCAP06(2007)023
- [14] F. Bernardeau and T. Brunier, *Non-Gaussianities in extended D-term inflation*, Phys. Rev. D **76** (2007) 043526.
- [15] N. Barnaby and J. M. Cline, *Large NonGaussianity from Nonlocal Inflation*, JCAP07(2007)017.
- [16] K. Koyama, S. Mizuno, F. Vernizzi and D. Wands, *Non-Gaussianities from ekpyrotic collapse with multiple fields*, JCAP11(2007)024.
- [17] R. Holman and A. J. Tolley, *Enhanced Non-Gaussianity from Excited Initial States*, JCAP 0805(2008)001.
- [18] J. Khoury and F. Piazza, *Rapidly-Varying Speed of Sound, Scale Invariance and Non-Gaussian Signatures*, JCAP 0907(2009)026.
- [19] A. Ashoorioon and G. Shiu, *A Note on Calm Excited States of Inflation*, JCAP 03(2011)025.
- [20] E. Komatsu et al., *First Year Wilkinson Microwave Anisotropy Probe (WMAP) Observations: Tests of Gaussinity*, Astrophys. J. Supp. **148** (2003) 119.
- [21] P. Creminelli, A. Nicolis, L. Senatore, M. Tegmark and M. Zaldarriaga, *Limits on non-Gaussianities from WMAP data*, JCAP 05(2006)004.
- [22] P. Creminelli, L. Senatore, M. Tegmark and M. Zaldarriaga, *Limits on f_{NL} from WMAP 3yr data*, JCAP03(2007)005.
- [23] A. P. S. Yadav and B. D. Wandelt, *Detection of primordial non-Gaussianity (f_{NL}) in the WMAP 3-year data at above 99.5% confidence*, Phys. Rev. Lett. **100** (2008) 181301.
- [24] D. Babich, P. Creminelli and M. Zaldarriaga, *The shape of non-Gaussianities*, JCAP 08(2004)009.
- [25] P. Creminelli, L. Senatore and M. Zaldarriaga, *Estimators for local non-Gaussianities*, JCAP 0703(2007)019.
- [26] J. R. Fergusson and E. P. S. Shellard, *The shape of primordial non-Gaussianity and the CMB bispectrum*, Phys. Rev. D **80** (2009) 043510.
- [27] P. D. Meerburg, J. P. Van der Schaar and P. S. Corasaniti, *Signatures of Initial State Modifications on Bispectrum Statistics*, JCAP 0905(2009)018.
- [28] J. N. Fry and R. J. Scherrer, *Skewness and nongaussian initial conditions*, Astrophys. J. **429** (1994) 36.

- [29] R. Durrer, R. Juszkiewicz, M. Kunz and J.-P. Uzan, *Skewness as a probe of non-gaussian initial conditions*, Phys. Rev. D **62** (2000) 021301.
- [30] H. A. Feldman, J. A. Frieman, J. N. Fry and R. Scoccimarro, *Constraints on galaxy bias, matter density, and primordial non-Gaussianity from the PSCZ galaxy redshift survey*, Phys. Rev. Lett. **86** (2001) 1434.
- [31] R. Scoccimarro, E. Sefusatti and M. Zaldarriaga, *Probing primordial non-Gaussianity with large-scale structure*, Phys. Rev. D **69** (2004) 103513.
- [32] E. Sefusatti and E. Komatsu, *The bispectrum of galaxies from high-redshift galaxy surveys: primordial non-Gaussianity and non-linear galaxy bias*, Phys. Rev. D **76** (2007) 083004.
- [33] F. Lucchin and S. Matarrese, *The effect of non-Gaussian statistics on the mass multiplicity of cosmic structures*, Astrophys. J. **330** (1988) 535.
- [34] S. Colafrancesco, F. Lucchin and S. Matarrese, *The mass function from local density maxima - Groups and clusters of galaxies*, Astrophys. J. **345** (1989) 3.
- [35] W.A. Chiu, J.P. Ostriker and M.A. Strauss, *Using Cluster Abundances and Peculiar Velocities to Test the Gaussianity of the Cosmological Density Field*, Astrophys. J. **494** (1998) 479.
- [36] V. Desjacques, U. Seljak and I. T. Iliev, *Scale-dependent bias induced by local non-Gaussianity: a comparison to N-body simulations*, Mont. Not. Roy. Astron. Soc. **396** (2009) 85.
- [37] M. Grossi et al., *Large-scale non-Gaussian mass function and halo bias: test on N-body simulations*, Mont. Not. Roy. Astron. Soc. **398** (2009) 321.
- [38] A. Pillepich, C. Porciani and O. Hahn, *Halo mass function and scale-dependent bias from N-body simulations with non-Gaussian initial conditions*, Mont. Not. Roy. Astron. Soc. **402** (2010) 191.
- [39] C. Wagner, L. Verde and L. Boubekur, *N-body simulations with generic non-Gaussian initial conditions I: power spectrum and halo mass function*, JCAP10(2010)022.
- [40] W. H. Press and P. Schechter, *Formation of Galaxies and Clusters of Galaxies by Self-Similar Gravitational Condensation*, Astrophys. J. **187** (1974) 425.
- [41] J. E. Gunn and J. R., Gott III, *On the Infall of Matter Into Clusters of Galaxies and Some Effects on Their Evolution*, Astrophys. J. **176** (1972) 1.
- [42] S. Matarrese, L. Verde and R. Jimenez, *The Abundance of High-Redshift Objects as a Probe of Non-Gaussian Initial Conditions*, Astrophys. J. **541** (2000) 10.
- [43] M. LoVerde, A. Miller, S. Shander and L. Verde, *Effects of scale-dependent non-Gaussianity on cosmological structures*, JCAP 04(2008)014.
- [44] T. Y. Lam and R. K. Sheth, *Halo abundances in the f_{nl} model*, Mont. Not. Roy. Astron. Soc. **398** (2009) 2143.
- [45] J. R. Bond, S. Cole, G. Efstathiou and G. Kaiser, *Excursion set mass functions for hierarchical Gaussian fluctuations*, Astrophys. J. **379** (1991) 440.
- [46] A. R. Zentner, *The Excursion Set Theory of Halo Mass Functions, Halo Clustering, and Halo Growth*, Int. J. Mod. Phys. D **16**, 763 (2007).

- [47] W.J. Percival, *The build-up of halos within Press-Schechter theory*, Mont. Not. Roy. Astron. Soc. **327** (2001) 1313.
- [48] M. Maggiore and A. Riotto, *The Halo Mass Function from Excursion Set Theory. I. Gaussian Fluctuations with Non-Markovian Dependence on the Smoothing Scale*, Astrophys. J. **711** (2010) 907 (2010).
- [49] M. Maggiore and A. Riotto, *The Halo mass function from Excursion Set Theory. II. The Diffusing Barrier* Astrophys. J. **717**, 515 (2010).
- [50] M. Maggiore and A. Riotto, *The Halo Mass Function from Excursion Set Theory. III. Non-Gaussian Fluctuations* Astrophys. J. **717**, 526 (2010).
- [51] P. S. Corasaniti and I. Achitouv, *Toward a Universal Formulation of the Halo Mass Function*, Phys. Rev. Lett. **106**, 241302 (2011)
- [52] P. S. Corasaniti and I. Achitouv, *Excursion Set Halo Mass Function and Bias in a Stochastic Barrier Model of Ellipsoidal Collapse*, Phys. Rev. D **84**, 023009 (2011).
- [53] E. Audit, R. Teyssier and J.-M. Alimi, *Non-linear dynamics and mass function of cosmic structures. I. Analytical results*, Astron. & Astrophys. **325** (1997) 439.
- [54] R. K. Sheth, H. J. Mo and G. Tormen, *Ellipsoidal collapse and an improved model for the number and spatial distribution of dark matter haloes*, Mont. Not. Roy. Astron. Soc. **323** (2001) 1.
- [55] R. K. Sheth and G. Tormen, *Large-scale bias and the peak background split*, Mont. Not. Roy. Astron. **308** (1999) 119.
- [56] G. D’Amico, M. Musso, J. Noreña and A. Paranjape, *An Improved Calculation of the Non-Gaussian Halo Mass Function*, JCAP 02(2011)01.
- [57] A. de Simone, M. Maggiore and A. Riotto, *Excursion set theory for generic moving barriers and non-Gaussian initial conditions*, Mont, Not. Roy. Astron. **412** (2011) 2587.
- [58] E. Komatsu et al., *Seven-Year Wilkinson Microwave Anisotropy Probe (WMAP) Observations: Cosmological Interpretation*, Astrophys. J. Supp. **192** (2011) 18.
- [59] U. Seljak and M. Zaldarriaga, *A Line of Sight Approach to Cosmic Microwave Background Anisotropies*, Astrophys. J. **469** (1996) 437.
- [60] A. G. Doroshkevich, *Spatial structure of perturbations and origin of galactic rotation in fluctuation theory*, Astrophysika **3** (1970) 175.
- [61] D. J. Eisenstein, A. Loeb, *An Analytical Model for the Triaxial Collapse of Cosmological Perturbations*, Astrophys. J. **439** (1995) 520.
- [62] V. Desjacques, *Environmental dependence in the ellipsoidal collapse model*, MNRAS **388** (2008) 638.
- [63] J. L. Tinker et al., *Toward a Halo Mass Function for Precision Cosmology: The Limits of Universality*, Astrophys. J. **688** (2008) 709.
- [64] B. Robertson, A. Kravtsov, J. Tinker and A. Zentner, *Collapse Barriers and Halo Abundance: Testing the Excursion Set Ansatz*, Astrophys. J. **696** (2009) 636.
- [65] L. Jounghun, *The relative abundance of isolated cluster as a probe of Dark energy*,

arXiv:1108.1712v1.